AIAA JOURNAL
Vol. 31, No. 2, February 1993

Review of Unsteady Aerodynamic Methods for Turbomachinery Aeroelastic and Aeroacoustic Applications

Joseph M. Verdon
United Technologies Research Center, East Hartford, Connecticut 06108

Introduction

THE unsteady aerodynamic analyses intended for turbomachinery aeroelastic and aeroacoustic predictions must be applicable over wide ranges of blade-row geometries and operating conditions and unsteady excitation modes and frequencies. Also, because of the large number of controlling parameters involved, there is a stringent requirement for computational efficiency. To date these requirements have been met only to a limited extent. As a result, aeroelastic and aeroacoustic design predictions are, for the most part, still based on the classical linearized unsteady aerodynamic analyses developed in the early 1970s.

During the past decade, significant advances in unsteady aerodynamic prediction capabilities have been achieved. In particular, researchers have developed efficient linearized analyses that account for the effects of important design features, such as real blade geometry, mean blade loading, and operation at transonic Mach numbers, on the unsteady aerodynamic response of the blading to imposed structural and external aerodynamic excitations. The improvements in physical modeling that such linearizations allow are motivating their current implementation into aeroelastic and aeroacoustic design prediction systems. Also, considerable progress has been made on developing time-accurate Euler and Navier-Stokes simulations of nonlinear unsteady flows through blade rows. Although not yet suitable for design use, such analyses offer opportunities for an improved understanding of the unsteady aerodynamic processes associated with blade vibration and noise generation. These recent advances in the theoretical and computational modeling of turbomachinery unsteady flows are reviewed in the present survey.

Blade Vibration and Noise Generation

The development of theoretical analyses to predict unsteady flows in axial-flow turbomachines has been motivated primarily by the need to predict the aeroelastic and the aeroacoustic behaviors of the blading. For both applications, an unsteady aerodynamic analysis is only one component of an overall design prediction system. However, because of the complexity of the unsteady fluid dynamic environment, this component has generally been regarded as the one requiring the most research attention.

Blade vibration and noise generation are both undesirable consequences of the unsteady flow processes that occur within an axial-flow turbomachine and are, therefore, important concerns to the designer. Of the two, vibration problems have received more attention because they can lead to a structural failure of the blading and, possibly, extensive damage to the engine. Although excessive noise can be disturbing and may in the future limit access to certain airports, the associated pressure fluctuations rarely threaten structural integrity.

Aerodynamically induced blade vibrations are usually classified into two general categories: flutter and forced vibration. In the former, the aerodynamic forces that sustain the blade motion are regarded as being dependent solely on that motion, whereas in the latter, the aerodynamic forces that excite the blade motion are independent of that motion. In both circumstances the vibratory motion of the blading can lead to fatigue failure. In modern fans and compressors flutter can be encountered over a wide range of operating conditions. The common types have been designated as classical supersonic (unstalled) flutter, subsonic/transonic high-incidence (or stalled) flutter, supersonic positive-incidence flutter, and negative-incidence or choke flutter. Classical supersonic flutter can occur at design operating conditions; the others occur at off-design conditions, with subsonic/transonic positive-incidence flutter having the highest frequency of occurrence.[1-3] Because of performance trends toward higher flow velocities, turbine flutter has also become an important concern.

Destructive forced vibrations can occur in fan, compressor, or turbine blading when a periodic aerodynamic excitation, with frequency close to a structural system natural frequency,

Joseph M. Verdon received his B.S. from Webb Institute of Naval Architecture in 1963 and his M.S. and Ph.D. in engineering science from the University of Notre Dame in 1965 and 1967, respectively. He has since taught courses in fluid dynamics and applied mechanics at the University of Connecticut and has spent two summers as a Faculty Fellow at NASA Langley Research Center. Since 1972, Dr. Verdon has been conducting research on turbomachinery aerodynamics at the United Technologies Research Center (UTRC). He is currently Manager, Theoretical and Computational Fluid Dynamics, with responsibility for research programs on unsteady aerodynamics, inviscid/viscid interaction theory, computational fluid dynamics, and blade-row aeroacoustics and aeroelastics. In 1988 he received a UTRC Special Award for the Advancement of Science and Technology. He has extensive research experience in unsteady aerodynamics and has contributed numerous journal articles and technical reports and prepared several survey articles on this field. He has also lectured extensively in the United States and overseas and served on Ph.D. thesis committees at various universities. Dr. Verdon is recognized as one of the pioneers in the development and application of analytical procedures for predicting and avoiding unstalled supersonic flutter in fan rotors and in the development of a general linearized unsteady aerodynamic theory for turbomachinery blade rows. He is an Associate Fellow of the AIAA and has recently completed a three-year term as an Associate Editor of the *AIAA Journal*. He is also a member of the Society for Industrial and Applied Mathematics, the Society of Sigma Xi, and the American Institute of Mechanical Engineers (ASME) and currently serves as a member of the ASME Gas Turbine Division, Structures and Dynamics Committee.

Presented as Paper 92-0011 at the AIAA 30th Aerospace Sciences Meeting, Reno, NV, Jan. 6-9, 1992; received March 2, 1992; revision received June 23, 1992; accepted for publication July 13, 1992.

acts on the blades in a given row. Such excitations are usually generated at multiples of the engine rotation frequency and arise from a variety of sources, including inlet and exit flow nonuniformities and the aerodynamic interactions that occur between a given blade row and neighboring blade rows or structural supports that move at a different rotational speed. The two principal types of such interaction are usually referred to as potential flow and wake interaction. The former is associated with pressure variations that impinge on a given array from upstream and/or downstream and is of serious concern when the axial spacings between neighboring blade rows are small or flow Mach numbers or excitation frequencies are high. Wake interaction is the effect on the flow through a given row of the wakes shed by one or more upstream rows and can persist over considerable axial distances.

External aerodynamic excitations also contribute to the noise generated by blade rows. Most of the research on turbomachinery noise has focused on the fan stage of modern high bypass ratio engines because the fan controls fly-over noise on landing approach and is a strong contributor along with jet noise at takeoff.[4] Typical spectra of the noise radiated from the inlet and exit of a fan operating at subsonic tip speed show tones at the rotor/stator blade-passing frequency and its harmonics and broadband noise at a lower level elsewhere. At supersonic tip speeds multiple pure tones or combination tones, associated with rotor-locked leading-edge shocks, also appear at the inlet at multiples of the shaft rotation frequency. The primary mechanisms responsible for pure tone noise are the wake and potential-flow interactions that occur between the various elements of the fan, i.e., the rotor, the exit guide vane (stator), and the supporting struts. Broadband noise is generated by the interaction of random disturbances, e.g., those associated with inlet boundary-layer and rotor-wake turbulence, with the downstream blading.

Unsteady Aerodynamic Analyses

The unsteady aerodynamic analyses intended for turbomachinery aeroelastic and aeroacoustic applications must be capable of predicting the aerodynamic responses of a blade row to prescribed structural (i.e., blade motions) and external aerodynamic excitations. The latter include variations in total pressure, total temperature, and static pressure at inlet and variations in static pressure at exit. For aeroelastic applications, the unsteady loads that act on the vibrating blades must be determined. For aeroacoustic applications, the pressure waves that carry energy away from the blade row are the response quantities of interest. Because of the large number of controlling parameters involved, the analyses must be capable of providing the necessary aerodynamic response information both efficiently and economically.

The unsteady aerodynamic analyses currently used in aeroelastic and aeroacoustic design applications are based on classical linearized inviscid flow theory (see Whitehead[5] for a review), which essentially applies to lightly loaded thin-airfoil cascades. Very efficient semi-analytic solution procedures have been developed for two-dimensional, attached, subsonic flows,[6-8] high-frequency transonic flows,[9] and supersonic flows with subsonic[10-14] or supersonic[15] axial velocity component. Models based on variations or extensions of the two-dimensional classical linearization have also been developed to treat separated subsonic flows[16,17] and supersonic flows with strong in-passage normal shocks.[18] Finally, extensive efforts have also been made to develop three-dimensional classical linearized analyses, as reviewed by Namba.[19]

The classical two-dimensional subsonic and supersonic analyses, supplemented by a good deal of empiricism, have been used for most current designs. Those for supersonic flow with subsonic axial velocity component have been very important because they have been found to give conservative estimates for the onset of supersonic unstalled torsional flutter in fans. Classical analyses provide very efficient unsteady aerodynamic response predictions that are useful near design operating conditions, but they are not appropriate off design, where blade loading effects are important, or for transonic flows with embedded shock discontinuities.

To overcome the limitations of the classical model, while retaining some measure of computational efficiency, general, two-dimensional, inviscid, unsteady aerodynamic linearizations have been developed.[20-22] Here, the unsteady flow is regarded as a small perturbation of a fully nonuniform compressible steady flow. Thus, the steady flow is governed by a nonlinear equation set; the unsteady flow, by a system of linear equations with variable coefficients that depend on the underlying steady flow. Unsteady linearizations relative to potential mean or steady background flows[23-31] have received considerable attention over the past decade, and linearized Euler analyses[32,33] are currently being developed to address unsteady flows containing strong shocks. Although solutions based on these analyses require significantly greater computing times than classical solutions, the improvements in physical modeling that they allow, coupled with advances in our ability to resolve numerically the resulting governing equation sets, are making this approach an increasingly attractive one for aeroelastic and aeroacoustic design applications.

Although linearized inviscid analyses meet the needs of turbomachinery designers for efficient unsteady aerodynamic response predictions, they do not account for potentially important unsteady flow phenomena, e.g., phenomena associated with finite amplitude excitation, viscous-layer displacement and separation, large shock excursion, etc. Thus, work has been proceeding to develop time-accurate, nonlinear, inviscid (Euler) and viscid (Reynolds-averaged Navier-Stokes) solution techniques for unsteady flows through isolated and aerodynamically coupled blade rows. Such analyses provide more comprehensive physical modeling capabilities, but they also require substantial computational resources.

Since the early 1980s, a number of Euler and Navier-Stokes procedures have been developed to address flows through single blade rows in which the unsteadiness is caused by blade vibration[34-43] or by aerodynamic disturbances at the inflow or outflow boundaries[44,45] and flows through aerodynamically coupled blade rows in which the unsteadiness is caused by the relative motions between the blade rows[46-52] and by aerodynamic disturbances at inlet.[53-55] The research on isolated cascades of vibrating blades has focused on fan and compressor flutter applications. Here, the Euler or Navier-Stokes equations are solved on time-dependent grids that deform with the blade motion. The methods for unsteady flows excited by external aerodynamic excitations or by the aerodynamic coupling between adjacent stationary and rotating blade rows treat blades that are fixed in the stator or rotor frame of reference. For the most part, such analyses have been applied to study wake/turbine rotor, turbine stator/rotor, or combustor hotstreak/turbine stator/rotor interactions.

This paper reviews the unsteady aerodynamic models that are currently being developed for turbomachinery blade rows. As a convenience, these models will be described for two-dimensional unsteady flows through isolated or single blade rows. The extensions required to treat three-dimensional flows and flows through coupled blade rows are, for the most part, reasonably straightforward, at least conceptually. The reader will determine that, although significant progress has been made, substantial future research will be required before fully acceptable unsteady aerodynamic analyses can be introduced into the turbomachinery aeroelastic and aeroacoustic design processes.

Unsteady Aerodynamic Problem

We consider time-dependent flow, with negligible body forces, of a perfect gas with constant specific heats through a two-dimensional cascade, such as the one shown in Fig. 1. The unsteady fluctuations in the flow arise from one or more of the following sources: blade motions, upstream total temperature and total pressure disturbances, and upstream and/or down-

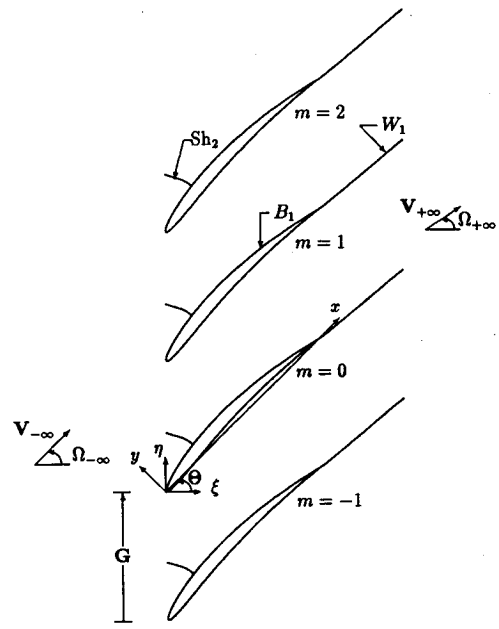

Fig. 1 Two-dimensional transonic compressor cascade; $M_{+\infty} < M_{-\infty} < 1$.

stream static pressure disturbances that carry energy toward the blade row. In the absence of unsteady excitation, the flow far upstream from the blade row is assumed to be at most a small steady perturbation from a uniform freestream. If the underlying mean flow is essentially uniform, then any arbitrary unsteady aerodynamic excitation of small amplitude can be represented approximately as the sum of independent entropic, vortical, and acoustic disturbances that travel toward the blade row, as indicated in Fig. 2.

In the present discussion all physical variables are dimensionless, most vector quantities are in boldface type, and a tilde over a dependent variable indicates time dependence. Lengths have been scaled with respect to blade chord, time with respect to the ratio of blade chord to upstream freestream flow speed, density with respect to the upstream freestream density, velocity with respect to the upstream freestream flow speed, and pressure with respect to the product of the upstream freestream density and the square of the upstream freestream speed. The scalings for the remaining variables can be determined from the equations that follow, which are of the same form as their dimensional counterparts.

The mean or steady-state positions of the blade chord lines coincide with the line segments $\eta = \xi \tan\Theta + mG$, $0 \le \xi \le \cos\Theta$, $m = 0, \pm 1, \pm 2, \ldots$, where ξ and η are coordinates in the axial flow and cascade circumferential directions, respectively, m is a blade number index, Θ is the cascade stagger angle, and $\boldsymbol{G}$ is the cascade gap vector that is directed along the η axis with magnitude equal to the blade spacing. The blade motions, i.e.,

$$\mathcal{R}(\boldsymbol{x} + m\boldsymbol{G}, t) = \mathrm{Re}\left\{\boldsymbol{r}(\boldsymbol{x}) \exp\left[i(\omega t + m\sigma)\right]\right\}, \quad \boldsymbol{x} \in B \tag{1}$$

are prescribed functions of position $\boldsymbol{x}$ and time t. Here $\mathcal{R}$ is the displacement of a point on a moving blade surface ($\mathcal{B}_m$) relative to its mean or steady-state position (B_m), are prescribed functions of position $\boldsymbol{x}$ and time t. The $\boldsymbol{r}$ is the complex amplitude of the blade displacement, σ is the phase angle between the motions of adjacent blades, Re{ } denotes the real part of { }, and B denotes the reference ($m = 0$) blade.

The entropic, $\tilde{s}_{-\infty}(\boldsymbol{x}, t)$, vortical, $\tilde{\boldsymbol{\zeta}}_{-\infty}(\boldsymbol{x}, t)$, and acoustic, $\tilde{p}_{I,\mp\infty}(\boldsymbol{x}, t)$, excitations, where the subscripts $-\infty$ and $+\infty$ refer to regions far upstream ($\xi \le \xi_-$) and far downstream ($\xi \ge \xi_+$) from the blade row, respectively, are also prescribed functions of $\boldsymbol{x}$ and t. The conditions at inlet and exit must be compatible with the fluid dynamic field equations, and the prescribed pressure disturbances must be of the type that carry energy toward the blade row. Although more general situations can be accommodated, here we assume that the external aerodynamic excitations are steady in a reference frame that moves at constant velocity V_{EXC} in the η direction. Therefore, in the blade-row frame of reference, they are periodic in η with fundamental wave number $\kappa_\eta = \sigma G^{-1}$ and periodic in time with fundamental frequency $\omega = -\kappa_\eta V_{\mathrm{EXC}}$.

The equations that govern the flow are determined from the conservation laws for mass, momentum, and energy and the thermodynamic relations for a perfect gas. To describe unsteady flows it is convenient to express the conservation laws relative to an arbitrary moving control volume $\nu(t)$, which is bounded by the moving control surface $\mathcal{S}(\boldsymbol{x}, t)$, i.e.,

$$\frac{\mathrm{d}}{\mathrm{d}t}\int_{\mathcal{V}} \tilde{\rho}\,\mathrm{d}\mathcal{V} + \int_{\mathcal{S}} \tilde{\rho}(\tilde{\boldsymbol{V}} - \dot{\mathcal{R}}) \cdot \boldsymbol{n}\,\mathrm{d}\mathcal{S} = 0 \tag{2}$$

$$\frac{\mathrm{d}}{\mathrm{d}t}\int_{\mathcal{V}} \tilde{\rho}\tilde{\boldsymbol{V}}\,\mathrm{d}\mathcal{V} + \int_{\mathcal{S}} \tilde{\rho}\left[\tilde{\boldsymbol{V}} \otimes (\tilde{\boldsymbol{V}} - \dot{\mathcal{R}})\right] \cdot \boldsymbol{n}\,\mathrm{d}\mathcal{S} = \int_{\mathcal{S}} \tilde{\boldsymbol{T}} \cdot \boldsymbol{n}\,\mathrm{d}\mathcal{S} \tag{3}$$

and

$$\frac{\mathrm{d}}{\mathrm{d}t}\int_{\mathcal{V}} \tilde{\rho}\tilde{E}_T\,\mathrm{d}\mathcal{V} + \int_{\mathcal{S}} \tilde{\rho}\tilde{E}_T(\tilde{\boldsymbol{V}} - \dot{\mathcal{R}}) \cdot \boldsymbol{n}\,\mathrm{d}\mathcal{S} = \int_{\mathcal{S}} \tilde{\boldsymbol{V}} \cdot \tilde{\boldsymbol{T}} \cdot \boldsymbol{n}\,\mathrm{d}\mathcal{S} - \int_{\mathcal{S}} \tilde{\boldsymbol{q}} \cdot \boldsymbol{n}\,\mathrm{d}\mathcal{S} \tag{4}$$

where $\tilde{\rho}$, $\tilde{\boldsymbol{V}}$, and $\tilde{E}_T = \tilde{E} + \tilde{\boldsymbol{V}}^2/2$ are the fluid density, velocity, and specific total internal energy, respectively, $\mathcal{R}(\boldsymbol{x}, t)$ defines the displacement of points on the control surface, $\dot{\mathcal{R}} = \partial\mathcal{R}/\partial t|_{\boldsymbol{x}}$, $\tilde{\boldsymbol{T}}$ is the stress tensor, $\tilde{\boldsymbol{q}}$ is the heat flux vector, $\boldsymbol{n}$ is a unit outward normal vector, and $\otimes$ denotes the tensor or dyadic product. For a Newtonian fluid having zero coefficient of bulk viscosity, the stress tensor (dyadic) is related to the fluid (thermostatic) pressure $\tilde{P}$ and velocity $\tilde{\boldsymbol{V}}$ by

$$\tilde{\boldsymbol{T}} = -\tilde{P}\boldsymbol{I} - \tilde{\mu}Re^{-1}\left[(2\nabla \cdot \tilde{\boldsymbol{V}}/3)\boldsymbol{I} - \nabla \otimes \tilde{\boldsymbol{V}} - (\nabla \otimes \tilde{\boldsymbol{V}})_c\right] \tag{5}$$

where $\boldsymbol{I}$ is the unit tensor, $\tilde{\mu}$ is the coefficient of shear viscosity, $Re = \rho^* V^* L^*/\mu^*$ is the flow Reynolds number, the superscript * refers to a dimensional reference value of a flow variable, and the subscript c denotes the conjugate dyadic. The heat flux $\tilde{\boldsymbol{q}}$ is related to the gradient of temperature via Fourier's law, i.e., $\tilde{\boldsymbol{q}} = -\tilde{k}Pr^{-1}Re^{-1}\nabla\tilde{T}$, where $\tilde{k}$ is the coefficient of thermal conductivity, $Pr = \mu^* C_p^*/k^*$ is the Prandtl number of the flow, and C_p^* is the specific heat of the fluid at constant pressure. The coefficients $\tilde{\mu}$ and $\tilde{k}$ are assumed to be known functions of the temperature $\tilde{T}$.

In addition to the foregoing equations, two relations from classical thermodynamics are also required, in particular, the equation of state for a thermally perfect gas and the equation

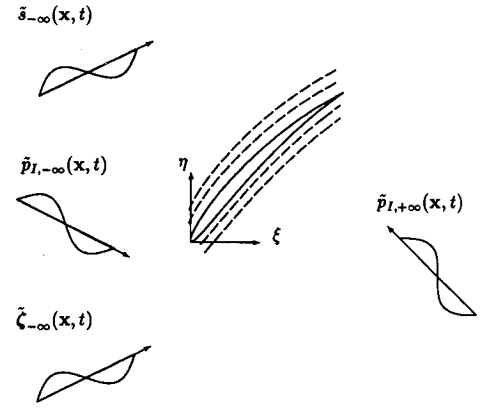

Fig. 2 Unsteady excitations: blade motion, incident vortical and entropic disturbances from upstream, and incident acoustic disturbances from upstream and downstream.

relating the internal energy and the temperature for a calorically perfect gas, i.e.,

$$\tilde{P} = \gamma^{-1}(\gamma-1)\tilde{\rho}\tilde{T} \quad \text{and} \quad \tilde{E} = \gamma^{-1}\tilde{T} = (\gamma-1)^{-1}\tilde{P}/\tilde{\rho} \tag{6}$$

respectively, where γ is the specific heat ratio of the fluid (constant pressure to constant volume). It is also useful to introduce the fundamental thermodynamic identity

$$d\tilde{S} = T^{-1}\left[d\tilde{E} + \tilde{P}d(\tilde{\rho}^{-1})\right] = \gamma^{-1}\frac{d\tilde{P}}{\tilde{P}} - \frac{d\tilde{\rho}}{\tilde{\rho}} \tag{7}$$

where $\tilde{S}$ is the specific entropy of the fluid.

Nonlinear Unsteady Aerodynamic Analyses

The foregoing equations provide a sufficient set for determining the unknown fluid-dynamic variables. For turbulent flows these equations describe the behavior of the ensemble- or Reynolds-averaged values of the time-dependent flow variables. The effects of random turbulent fluctuations are accommodated by including turbulent velocity correlations in the definition of the stress tensor $\tilde{T}$. To obtain closure of the mean flow equations, these correlations are usually related to gradients in the ensemble-averaged or mean-flow velocity components via algebraic eddy viscosity models.

Viscous Flow—Navier-Stokes Equations

Equations that describe the fluid motion at a moving field point, $\tilde{x} = x + \Re(x, t)$, are obtained from the integral conservation laws by applying the transport theorem to interchange the order of time differentiation and volume integration, by applying Green's theorem to convert the surface integrals to volume integrals, and by taking the limit of the resulting expressions as $\mathcal{V}(t) \to 0$.[56] We find that

$$\left.\frac{\partial\tilde{\rho}}{\partial t}\right|_{\tilde{x}} + \tilde{\rho}\nabla\cdot\dot{\tilde{x}} + \nabla\cdot\left[\tilde{\rho}(\tilde{V}-\dot{\tilde{x}})\right] = 0 \tag{8}$$

$$\left.\frac{\partial}{\partial t}(\tilde{\rho}\tilde{V})\right|_{\tilde{x}} + \tilde{\rho}\tilde{V}(\nabla\cdot\dot{\tilde{x}}) + \nabla\cdot\left[\tilde{\rho}(\tilde{V}-\dot{\tilde{x}})\otimes\tilde{V}\right] = \nabla\cdot\tilde{T} \tag{9}$$

and

$$\left.\frac{\partial}{\partial t}(\tilde{\rho}\tilde{E}_T)\right|_{\tilde{x}} + \tilde{\rho}E_T\nabla\cdot\dot{\tilde{x}}\nabla\cdot\left[\tilde{\rho}(\tilde{V}-\dot{\tilde{x}})\tilde{E}_T\right] = \nabla\cdot(\tilde{V}\cdot\tilde{T}) - \nabla\cdot\tilde{q} \tag{10}$$

These (conservation) forms of the Reynolds-averaged Navier-Stokes equations correspond to the integral forms, Eqs. (2–4), and are usually preferred in numerical simulations, but the convective forms, i.e.,

$$\frac{D\tilde{\rho}}{Dt} + \tilde{\rho}\nabla\cdot\tilde{V} = 0 \tag{11}$$

$$\tilde{\rho}\frac{D\tilde{V}}{Dt} - \nabla\tilde{T} = 0 \tag{12}$$

and

$$\tilde{\rho}\frac{D\tilde{S}}{Dt} = \tilde{T}^{-1}\left[\tilde{P}\nabla\cdot\tilde{V} + \tilde{T}:(\nabla\otimes\tilde{V})1w - \nabla\cdot\tilde{q}\right] \tag{13}$$

are also useful. Here, $D/Dt = \partial/\partial t|_{\tilde{x}} + (\tilde{V}-\dot{\tilde{x}})\cdot\nabla = \partial/\partial t|_x + \tilde{V}\cdot\nabla$ is the material or convective derivative operator, and the notation : signifies the scalar product of two tensors. The entropy transport equation, Eq. (13), is obtained by combining Eqs. (10–12) and the fundamental thermodynamic identity (7) and performing the necessary algebra.

For application to turbomachinery unsteady flows, the field equations must be supplemented by conditions at the vibrating blade surfaces and conditions at the inflow and outflow boundaries. Since transient unsteady aerodynamic behavior is usually not of interest, a precise knowledge of the initial state of the fluid is not required. The no-slip condition, i.e., $\tilde{V} = \dot{\Re}$ for $x \in \mathcal{B}_m$, where $\Re$ is prescribed, applies at blade surfaces. In addition, either the heat flux $\tilde{q}\cdot n$ or the temperature $\tilde{T}$ must be prescribed at such surfaces. The total pressure and total temperature fluctuations at inlet and the incident pressure fluctuations at inlet and exit must also be specified. The total pressure and total temperature fluctuations at exit and the unsteady pressure response at inlet and exit must be determined as part of the time-dependent solution.

The Navier-Stokes equations are needed if convective nonlinearities and viscous effects are expected to have an important impact on the unsteady aerodynamic response of a blade row. However, for many flows of practical interest the Reynolds number is usually sufficiently high so that the latter are concentrated in relatively thin layers across which the flow properties vary rapidly but continuously. These layers generally lie adjacent to the blade surfaces (boundary layers), downstream of the blades (wakes), and in the vicinity of rapid compressions (shocks). Separate sets of approximate equations, i.e., reduced forms of the Navier-Stokes equations, can be constructed and solved to describe the flows in the "outer" inviscid region and the "inner" viscid regions. Appropriate methods for coupling the inviscid and viscid solutions are also needed. If viscous effects are negligible, i.e., if $Re \to \infty$, it is sufficient to consider only the outer or inviscid flow.

Inviscid Flow—Euler Equations

In the inviscid limit the thicknesses of the viscous layers become zero, and they can be modeled as surfaces across which the flow variables are discontinuous. In particular, boundary layers and wakes become vortex sheets that support a discontinuity in tangential velocity, and shocks become surfaces that support a discontinuity in normal velocity. It is usually assumed that the boundary layers remain attached to the blade surfaces and support jumps in velocity from zero at the "walls" to inviscid values at their "edges." Furthermore, the vortex-sheet unsteady wakes emanate from the blade trailing edges and extend infinitely far downstream. The integral forms of the conservation laws are required to describe the flow over the entire domain of interest. These provide differential equations in regions where the flow variables are continuously differentiable and "jump" conditions at the surfaces across which the flow variables are discontinuous.

The field equations that govern continuous, inviscid, fluid motion (i.e., the Euler equations) are obtained from Eqs. (8–10) or (11–13) by setting $\tilde{T} = -\tilde{P}I$ and $\tilde{q} = 0$. These equations must be supplemented by jump conditions that apply across moving boundary layers $\mathcal{B}_m$, wakes $\mathcal{W}_m$, and shocks $\mathcal{S}_{m,n}$. Here the subscript n refers to the nth shock associated with the mth blade. The far-field conditions used in the inviscid approximation are the same as those indicated earlier for Navier-Stokes simulations.

The inviscid surface conditions are obtained from the integral conservation laws, Eqs. (2–4), by setting $\tilde{T} = -\tilde{P}I$ and $\tilde{q} = 0$, considering a control volume that contains an element of a surface of discontinuity, and taking the limit as this volume collapses into the surface element. The resulting conditions for conserving mass, momentum, and energy at a moving surface are

$$[\![\tilde{M}_f]\!] = 0 \tag{14}$$

$$\tilde{M}_f\,[\![\tilde{V}]\!] + [\![\tilde{P}]\!]\,n = 0 \tag{15}$$

and

$$\tilde{M}_f\,[\![\tilde{E}_T]\!] + [\![\tilde{P}\tilde{V}]\!]\,n = 0 \tag{16}$$

respectively, where $[\![\ ]\!]$ denotes the difference in a flow quantity across a surface of discontinuity, and

$$\tilde{M}_f = \tilde{\bar{\rho}}(\tilde{V} - \dot{\mathcal{R}}) \cdot \boldsymbol{n} \tag{17}$$

is the fluid mass flux across the moving surface.

Since vortex sheets support a jump in tangential velocity, i.e., $[\![V]\!] \cdot \tau \neq 0$, it follows from Eq. (15) that there is no mass flow across such surfaces. Hence, the conditions

$$\tilde{M}_f = 0, \quad [\![\tilde{P}]\!] = 0, \text{ and } [\![\tilde{V}]\!] \cdot \boldsymbol{n} = 0 \text{ for } \boldsymbol{x} \in \mathcal{B}_m \text{ or } \mathcal{W}_m \tag{18}$$

prevail at vortex sheet boundary-layer and wake surfaces. The first of these applies at the "outer edges" of the viscous layers and, therefore, also at the solid blade surfaces (the inviscid flow tangency condition). At shocks, $\tilde{M}_f \neq 0$; so it follows from Eq. (15) that the tangential component of the fluid velocity $\tilde{V}_\tau$ must be continuous. The remaining jump conditions, along with the thermodynamic equations of state, are then required to determine the shock velocity $\dot{\mathcal{R}}$ and the changes in the properties of the fluid as it passes through a shock. The surface displacement vector $\mathcal{R}(\boldsymbol{x}, t)$ is prescribed at blade surfaces, but at wake and shock surfaces it must be determined as part of the time-dependent solution.

Although the viscous displacement and curvature effects associated with actual boundary layers, wakes, and shocks are neglected in a purely inviscid analysis, changes could be made in the foregoing jump conditions to accommodate them. If so, the inviscid "outer" region solution could be matched to viscid "inner" region solutions to provide a solution for the complete flowfield. We refer the reader to the articles by Melnik[57] and Lock and Firmin[58] for comprehensive reviews on the application of such viscid/inviscid interaction concepts in steady-state aerodynamics.

Numerical Simulations

Extensive research has been conducted in recent years to develop time-accurate Euler and Reynolds-averaged Navier-Stokes solution procedures for unsteady flows through turbomachinery blade rows. These procedures build on schemes developed earlier for steady flows in which a sequence of iterative solutions are marched forward in "pseudotime" until a converged steady state is determined. The calculations for periodic unsteady flows are marched forward in "real" time from an initial steady state to a converged periodic unsteady state. Existing algorithms invariably treat the conservative forms of the nonlinear field equations in which the unknown variables are $\tilde{\bar{\rho}}$, $\tilde{\bar{\rho}}V$, and $\tilde{\bar{\rho}}\tilde{E}_T$. The field equations are solved subject to boundary conditions at the blade surfaces, e.g., the no-slip condition for viscous flows or the flow tangency condition for inviscid flows. However, shock- and wake-jump conditions are usually not imposed in inviscid calculations. Instead, shock and wake phenomena are "captured" by approximating the conservative forms of the field equations across surfaces of discontinuity. This tends to smear shock and wake behavior but considerably simplifies the numerical effort.

The governing equations are approximated using finite volume, finite difference, or finite element spatial discretizations, and the numerical solutions are advanced in time using single or multistage explicit or implicit time-marching procedures. Explicit schemes are favored for inviscid flows and implicit schemes for viscous flows because the high mesh densities required impose stringent constraints on the stability of explicit time-marching schemes. Inviscid solutions are usually determined on sheared H-type grids that cover an extended blade-passage solution domain (Fig. 3). For viscous calculations, "inner" O or C grids that wrap around the blades are used in conjunction with the "outer" H grids. To simulate blade motion, the meshes are made to deform so that the computational boundaries coincide with the physical blade boundaries at all instants of time. In viscous calculations the effects of turbulence are represented by the inclusion of a turbulence model, usually one of the algebraic eddy-viscosity models[59,60] widely used in steady flow calculations. Transition is assumed to occur instantaneously at specified discrete locations on the blade surfaces.

There are two weaknesses associated with algebraic turbulence models. First, they require extensive "fine tuning" to accurately predict eddy viscosities in regions of separation and in wakes. Second, the local turbulent viscosity is based on the instantaneous local velocity profile; hence, they do not account for the "history" effects associated with the temporal or spatial development of the unsteady flow. The use of one- or two-equation turbulence models has been suggested[50-52] to overcome these weaknesses.

In addition to the limitations placed on the solutions by the use of simple turbulence and transition models, two other simplifications are usually introduced that limit the nonlinear prediction capabilities of current time-marching analyses. These involve the conditions imposed at the inflow and outflow boundaries and the use of a time-lagged circumferential periodicity condition to relate the flows in adjacent blade passages. For steady flows the usual procedure is to specify the total pressure, the total enthalpy, and the flow direction at inlet and the static pressure at exit. Compatibility relations, one upstream and three downstream, are then applied along with the prescribed inlet and exit information to compute the flow variables at the inflow and outflow boundaries. Also, the steady flows produced under uniform inflow conditions will exhibit blade-to-blade periodicity, i.e., $F(\boldsymbol{x} + m\boldsymbol{G}) = F(\boldsymbol{x})$, $m = 0 \pm 1, \pm 2, \ldots$, where F is any steady fluid property. Thus, the solution domain can be restricted to a single, extended, blade-passage region.

For unsteady flows the incoming disturbances must be prescribed as functions of $\boldsymbol{x}$ of t that are compatible with the nonlinear equations of motion. The inlet and exit conditions must also allow disturbance waves that leave the solution domain, i.e., pressure response waves, and entropy and vorticity waves at exit, to pass through the boundaries without producing artificial reflections. At present, linearized, one-dimensional, characteristic theory is usually applied to provide inlet and exit conditions for nonlinear unsteady flow calculations. The assumption is made that the unsteady perturbations are plane waves with minimal variation in the circumferential direction. Entropic, vortical, and incoming pressure perturbations are specified at the inlet boundary, and the outgoing pressure characteristic is extrapolated from the interior of the solution domain. The incoming pressure perturbation is specified at the outlet boundary, and the entropic, vortical, and outgoing pressure characteristics are extrapolated from the interior. Thus, linear unsteady inlet and exit conditions are imposed in nonlinear unsteady flow calculations. Since these are based on one-dimensional characteristic theory, they are not strictly nonreflecting. Approximate, linear, two-dimensional, nonreflecting, inlet and exit conditions have been proposed,[61] but these have not yet been widely implemented into nonlinear unsteady flow codes.

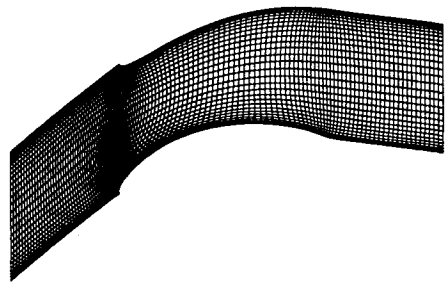

Fig. 3 Extended blade-passage solution domain and typical H grid used for unsteady flow calculations.

In general, the unsteady flows produced by circumferentially and temporally periodic unsteady excitations must be computed over many, and in some cases all, blade passages. The number of passages needed depends on the interblade phase angle $\sigma = \kappa_\eta G$ of the excitation. However, because multipassage calculations involve enormous computing times, a restrictive assumption is usually introduced to limit the computational domain to a single passage. Most investigators impose a phase-shifted periodicity condition, i.e., $\tilde{F}(x + mG, t - m\sigma/\omega) = \tilde{F}(x, t)$, $m = 0, \pm 1, \pm 2, \ldots$, where $\tilde{F}$ is any unsteady fluid property.[62] This condition implies that an unsteady excitation at wave number $\kappa_\eta = \sigma G^{-1}$ and frequency ω will produce a response at the same wave number and frequency, which is a valid consequence only for linear systems. It allows the solution domain to be restricted to a single blade-passage region, but a large amount of computer memory is still needed to store the unsteady flow variables at two periodic boundaries over an entire period of excitation.

Another approach for reducing the computational domain employs a dependent variable transformation to rewrite the governing equations in "time-inclined" computational coordinates.[45] This eliminates the storage requirements associated with phase-shifted periodicity but introduces additional complexity into the solution procedure for the interior flow. Also, whereas the phase-shifted periodicity condition imposes restrictions on the circumferential and temporal behavior of the unsteady response, time inclining places restrictions only on the circumferential behavior. Neither phase-shifted periodicity nor time inclining can be employed if excitations at different fundamental circumferential wave numbers occur simultaneously, for instance at the inlet and exit boundaries. In any case the use of these procedures places restrictions on the "nonlinear" response behavior that can be predicted.

Based on a review of the recent literature, the author estimates that 2500 grid points and 1000 time steps per cycle of excitation are used in a typical, single-passage, time-marching, Euler calculation. Five cycles are needed to converge the nonlinear inviscid solution to a periodic state, and the entire calculation requires about 10 CPU min on a Cray YMP. The corresponding numbers for a Navier-Stokes calculation are 12,500 mesh points per passage, 6000 time steps per cycle, 5 cycles to converge, and 3 CPU hours on a Cray YMP.

The number of grid points just cited are not sufficient to determine the first-harmonic or linear response, let alone the higher harmonic or nonlinear responses, in a number of important applications. These include the prediction of the onset transonic flutter and of the response of the blading to the aerodynamic excitations produced by an adjacent blade row.

For example, Giles[45] applied a time-marching Euler analysis to predict the response of a flat-plate cascade to a sinusoidal wake (vortical) excitation. This cascade has a gap-to-chord ratio G of 0.5 and a stagger angle Θ of 30 deg and operates

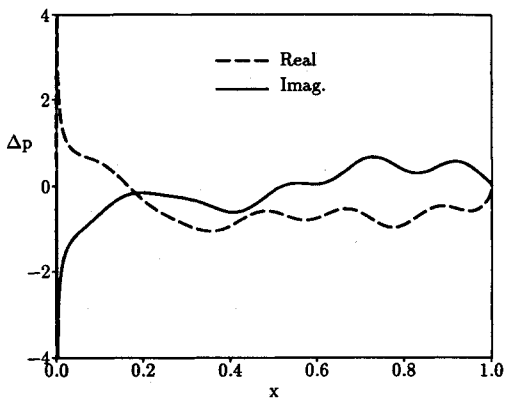

Fig. 4 Complex amplitude of the first-harmonic unsteady pressure difference acting on the reference blade of a flat-plate cascade ($G = 0.5$, $\Theta = \Omega_{-\infty} = 30$ deg, $M_{-\infty} = 0.7$) subjected to a harmonic wake excitation at $\omega = 13.96$ and $\sigma = -400$ deg.

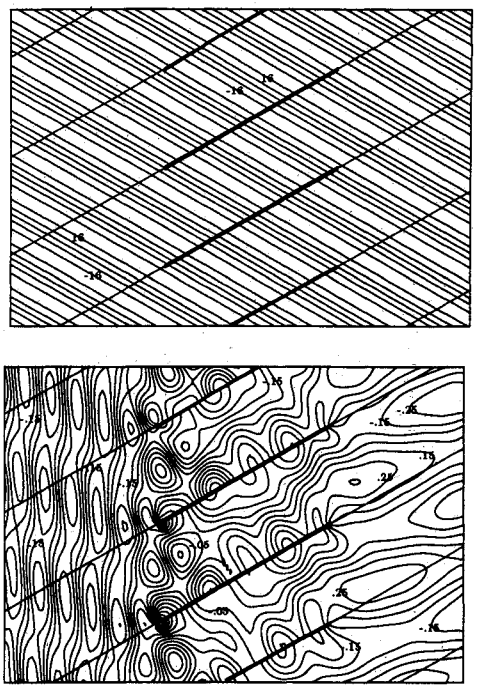

Fig. 5 In-phase components of the first-harmonic unsteady vorticity and unsteady pressure for a flat-plate cascade ($G = 0.5$, $\Theta = \Omega_{-\infty} = 30$ deg, $M_{-\infty} = 0.7$) subjected to a harmonic wake excitation with $\omega = 13.96$ and $\sigma = -400$ deg.

at an inlet Mach number $M_{-\infty}$ of 0.7 and flow angle $\Omega_{-\infty}$ of 30 deg. The frequency of the excitation is 13.96 and the interblade phase angle is -400 deg, corresponding to an incident wake to blade count ratio of 10/9. The complex amplitudes Δp of the first-harmonic, unsteady pressure differences, i.e., $\Delta\tilde{p} = \mathrm{Re}\{\Delta p \exp(i\omega t)\}$, acting along the reference blade surface, as determined using the classical linearized analysis of Smith,[6] are shown in Fig. 4. The real and imaginary parts of Δp represent the pressure differences that are in and out of phase, respectively, with the normal component of the vortical gust velocity at the leading edge of the reference blade. Excellent agreement was achieved between the numerical predictions of Ref. 45, which were determined using one-dimensional, nonreflecting, inlet and exit boundary conditions, and the classical theory prediction shown in Fig. 4, but the time-marching calculation required 18 cycles on a 200×25 H grid, followed by 12 cycles on a 400×50 grid.

Contours of the in-phase components of the first-harmonic unsteady vorticity and the unsteady pressure for this example, as determined using the linearized analysis of Ref. 30, are shown in Fig. 5. The vortical gust is convected, without distortion, by the uniform mean flow through the flat-plate blade row, but the interaction of this simple vortical field with the blading gives rise to a very complicated pressure (acoustic) response. The latter contains two propagating acoustic waves, at interblade phase angles of -40 and 320 deg that persist in both the far upstream and the far downstream regions of the flow. The strongest of these four waves travels upstream in a direction that is approximately normal to the inlet boundary. The others travel away from the blade row in directions that are approximately normal to or parallel with the inlet and exit boundaries. As a result a numerical calculation on a 400×50 grid in which one-dimensional inlet and exit conditions are applied seems to be adequate to predict the first-harmonic, inviscid, unsteady, pressure response.

It is easy, however, to construct a more difficult test case. For example, consider the same flat-plate cascade configuration, but with an incident disturbance to blade count ratio of 1.2, so that the excitation frequency and interblade phase angle are 15.08 and -432 deg, respectively. The vorticity contour

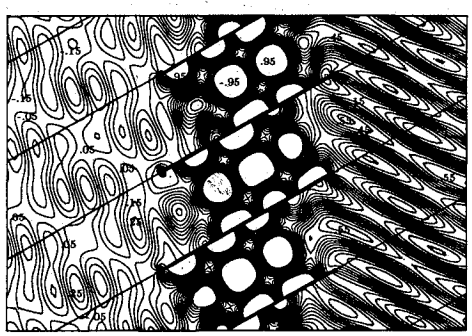

Fig. 6 In-phase component of the first-harmonic unsteady pressure for a flat-plate cascade ($G = 0.5$, $\Theta = \Omega_{-\infty} = 30$ deg, $M_{-\infty} = 0.7$) subjected to a harmonic wake excitation with $\omega = 15.08$ and $\sigma = -432$ deg.

pattern for this example is similar to that indicated in Fig. 5. Contours of the in-phase component of the first-harmonic unsteady pressure response are shown in Fig. 6. Very high unsteady pressure gradients occur within the blade passages, and three acoustic response disturbances at $\sigma = -74$, -288, and 648 deg persist far upstream and far downstream of the blade row. The far downstream disturbance at $\sigma = 648$ deg is quite strong, and its wave number vector, $\boldsymbol{k} = (k_\xi, k_\eta)$, is inclined at an angle of 64 deg measured counterclockwise from the axial flow direction. Because of the high unsteady gradients within the blade passage and the strong, oblique, propagating, pressure response downstream of the blade row, the resolution of this "relatively simple" unsteady flow would pose a very serious challenge to current time-marching, unsteady, fluid-dynamic analyses.

Recent Applications

In spite of the present limitations, very sophisticated, time-marching, nonlinear, unsteady aerodynamic analyses and codes have been developed and applied to realistic single and multiple blade-row configurations. Procedures for isolated cascades of vibrating blades have been developed for fan and compressor flutter applications. In these analyses, the Euler or Navier-Stokes equations are solved on grids that deform with time to account for the blade motion. Inviscid unsteady solutions have been determined for subsonic inlet flows[37,38] and for supersonic inlet flows with subsonic[39] or supersonic[40] axial velocity component. Since strong inviscid/viscid interaction effects are important in fan and compressor flows, a coupled Euler/integral boundary-layer method[41] has been developed to efficiently account for such interactions. In addition, a time-marching, Reynolds-averaged, Navier-Stokes solution procedure has been developed[42,43] to account more accurately for the effects of viscous-layer separation on the aerodynamic response to compressor blade vibrations.

Several research groups have developed methods for unsteady flows excited by incident aerodynamic excitations or by the aerodynamic coupling between adjacent stationary and rotating blade rows. Here the blades are fixed in the stator or rotor frame of reference, and the incident excitations or the relative motions between the adjacent rows give rise to high-frequency unsteady flows that can excite a forced blade vibration and/or discrete-tone noise propagation. The analyses have been applied to study wake/turbine rotor, turbine stator/turbine rotor, or combustor hotstreak/turbine stator/turbine rotor interactions. Euler calculations of wake/rotor interactions have been performed[44,45] in which incoming wakes were specified at the inflow boundaries of single turbine blade rows. The flow in the wakes was assumed to be parallel with uniform pressure and total enthalpy and a prescribed velocity defect distribution. Inviscid stator/rotor interactions have been calculated in three dimensions,[46] quasi-three dimensions,[47] and two dimensions.[48,49] In particular, two-dimensional calculations for a highly loaded transonic first turbine stage[49] have shown that the propagation and reflection of the shocks that originate at the trailing edge of the upstream stator can produce a 40% variation in the lift on the downstream rotor.

Perhaps the most well-known solutions for coupled blade rows are those based on the Reynolds-averaged Navier-Stokes calculations performed by Rai for stator/rotor interactions in two[50] and three[51] dimensions. Rai's method is actually a hybrid Navier-Stokes/Euler method in which the thin-layer Navier-Stokes equations are solved on an inner O grid, and the Euler equations are solved on an outer H grid. Recently, Giles and Haimes[52] have also provided such a hybrid analysis. Finally, Navier-Stokes solutions for the migration of a combustor hotstreak through an isolated turbine stage (stator and rotor) have been determined by several investigators.[53-55]

The time-accurate, nonlinear, unsteady flow analyses have been applied to flat-plate cascades so that nonlinear predictions could be compared with those of classical linearized theory. In general, the time-accurate results for subsonic flows are in very good agreement with those of classical linearized theory, but problems exist for superresonant subsonic flows,[38] i.e., subsonic flows in which an acoustic response persists in the far field of the blade row. For supersonic flows, the time-accurate surface-pressure predictions[39,40] are in qualitative agreement with those of classical theory, but the former indicate smeared oblique shocks and contain spurious blade-surface pressure variations in the regions between shock discontinuities. The time-accurate nonlinear analyses have also been applied to very challenging fan, compressor, and turbine flows. Reasonable steady and unsteady flow predictions that are in qualitative agreement with experimental measurements have been determined. However, reasons for the differences between the predictions and the measurements have not been firmly established.

The time-marching codes, although much too expensive at present for use in design, are receiving a great deal of attention. They are important because they give researchers a possible means for investigating and understanding nonlinear and viscous unsteady aerodynamic phenomena. Therefore, they can serve a useful role in determining the impact of transonic, viscous separation, and finite amplitude unsteady excitation effects on the aeroelastic and aeroacoustic response of blade rows.

Linearized Unsteady Aerodynamic Analyses

The computational resources required to simulate nonlinear inviscid and viscid unsteady fluid dynamic behavior will continue to prohibit the use of such simulations for aeroelastic or aeroacoustic design. Therefore, approximate analyses, based, for example, on the high Reynolds number flow and small unsteady disturbance assumptions, are still needed to provide efficient predictions of unsteady aerodynamic response phenomena. A significant advantage offered by a linearized inviscid approximation is that the first-order unsteady fluid motions arising from various Fourier modes of unsteady excitation are not coupled. Hence, it is sufficient to develop solution procedures for a single harmonic (in t and η) component of a given excitation. Solutions for arbitrary periodic excitations and arbitrary combinations of such excitations can then be obtained by superposition.

For small-amplitude unsteady excitations [i.e., $|r|$, $|\zeta_{-\infty}|$, etc., $\approx \mathcal{O}(\epsilon) \ll 1$] the time-dependent inviscid flow can be regarded as a small perturbation of an underlying nonlinear mean or steady background flow. Thus, for example, the nonlinear time-dependent fluid velocity $\tilde{\boldsymbol{V}}(\boldsymbol{x}, t)$ can be expressed as

$$\tilde{\boldsymbol{V}}(\boldsymbol{x}, t) = \boldsymbol{V}(\boldsymbol{x}) + \tilde{\boldsymbol{v}}(\boldsymbol{x}, t) + \cdots \tag{19}$$

where $\boldsymbol{V}(\boldsymbol{x})$ is the local mean velocity, $\tilde{\boldsymbol{v}}(\boldsymbol{x}, t)$ is the first-order (in ϵ) unsteady velocity, and $\boldsymbol{x}$ refers to a stationary point in the field. In addition, Taylor series expansions, e.g.,

$$\tilde{\boldsymbol{V}}_S = (\tilde{\boldsymbol{V}} + \mathcal{R} \cdot \nabla \tilde{\boldsymbol{V}} + \cdots)|_S \tag{20}$$

and surface-vector relations, i.e.,

$$\tau_{\mathcal{S}} = \tau_S + \left(n_S \cdot \frac{\partial \mathcal{R}}{\partial \tau_S}\right) n_S = \cdots \text{ and } n_{\mathcal{S}} = n_S - \left(\tau_S \cdot \frac{\partial \mathcal{R}}{\partial \tau_S}\right) \tau_S + \cdots \tag{21}$$

where $n \times \tau$ points out from the page, can be applied to refer information at a moving ($\mathcal{S}$) blade, wake, or shock surface to the mean (S) position of this surface.

Equations for the steady and first-order unsteady flow properties are determined by substituting the foregoing expansions into the full time-dependent Euler equations, equating terms of like power in ϵ and neglecting terms of $\mathcal{O}(\epsilon^2)$ or higher. The first-order or linearized unsteady response to a harmonic unsteady excitation at temporal frequency ω and circumferential wave number $\kappa_\eta = \sigma G^{-1}$ will be harmonic in time, e.g., $\tilde{v}(x, t) = \mathrm{Re}\{v(x) \exp(i\omega t)\}$, and will satisfy a phase-lagged, blade-to-blade, periodicity condition, e.g., $v(x + mG) = v(x) \exp(im\sigma)$. Thus, a solution to a time-independent, but complex, linearized unsteady flow problem is required only over a single extended blade-passage region of the cascade. In addition, since analytic far-field solutions can be determined,[63] the numerical solution domain can be restricted to a single extended blade-passage region of finite extent in the axial flow direction.

The field equations that govern the inviscid zeroth-order or steady background flow follow from those given previously, i.e., Eqs. (8–10) or (11–13), after setting $\tilde{T} = -\tilde{P}I$ and $\tilde{q} = 0$, replacing the nonlinear time-dependent flow variables, $\tilde{V}$, $\tilde{P}$, $\tilde{\rho}$, $\tilde{S}$, etc., by their zeroth-order counterparts, V, P, $\bar{\rho}$, S, etc., and setting local temporal derivatives $\partial/\partial t$ and surface displacements $\mathcal{R}$ equal to zero. Surface conditions for the zeroth-order or steady flow follow from Eqs. (14–17). Since $\mathcal{R} = 0$, these conditions are imposed at the mean positions of the blade, wake, and shock surfaces. Blade mean positions B_m are prescribed, but the mean wake W_m and shock $\mathrm{Sh}_{m,n}$ locations must be determined as part of the steady solution. Since the steady flow remains attached to the mean blade surfaces, $V \cdot n = 0$ for $x \in \mathrm{B}_m$. Also, the steady pressure and normal velocity component must be continuous across blade wakes, and mass, momentum, and energy must be conserved at the mean shock locations. Note that, if a strong shock impinges on a blade, the entropy and the tangential component of the fluid velocity will be discontinuous across its wake.

In addition to the foregoing surface conditions, conditions must be imposed on the steady flow far from the blade row. If the departures from uniform flow conditions in the far field are due solely to the presence of the blade row, the usual practice is to specify the total pressure, total enthalpy, and the direction of the uniform inlet flow and the static pressure of the exit flow. Small steady departures from these uniform flow conditions are determined as part of the nonlinear mean-flow solution.

Linearized Unsteady Equations

The linearized unsteady flow can be described via the conservative or convective forms of the differential field equations. Here we select the convective forms. Then, after introducing the first-order thermodynamic relation $s = \gamma^{-1} p/P - \rho/\bar{\rho}$, which follows from Eq. (7), to eliminate the density ρ, and performing the necessary algebra, we find that the first-order unsteady perturbation of a rotational and nonisentropic, steady flow is described by the following system of linearized Euler equations:

$$\frac{\bar{\mathrm{D}}s}{\mathrm{D}t} + v \cdot \nabla S = 0 \tag{22}$$

$$\frac{\bar{\mathrm{D}}}{\mathrm{D}t}(v - sV/2) + \left[(v - sV/2) \cdot \nabla\right] V + \nabla(p/\bar{\rho}) + \frac{V}{2}\frac{\bar{\mathrm{D}}s}{\mathrm{D}t} - \bar{\rho}^{-1} p \nabla S = 0 \tag{23}$$

and

$$\frac{\bar{\mathrm{D}}}{\mathrm{D}t}\left[p/(\bar{\rho}A^2) - s\right] + \bar{\rho}^{-1} \nabla \cdot (\bar{\rho} v) = 0 \tag{24}$$

Here s, v, and p are the complex amplitudes of the first-order entropy, velocity, and pressure, respectively, and $\bar{\mathrm{D}}/\mathrm{D}t = i\omega + V \cdot \nabla$ is a convective derivative operator based on the mean flow velocity. The linearized unsteady flow can be determined by solving Eqs. (22–24), subject to the appropriate surface and far-field conditions.

The linearized flow tangency condition follows from Eq. (18) and is given by

$$v \cdot n = \left[i\omega r + (V \cdot \tau)(\tau \cdot \nabla) r - (r \cdot \nabla) V\right] \cdot n, \quad x \in \mathrm{B}_m \tag{25}$$

The linearized wake-jump conditions also follow from Eq. (18) and can be expressed in the form

$$[\![p]\!] = -\kappa r \cdot n \left[\!\left[\bar{\rho}(V \cdot \tau)^2\right]\!\right], \qquad x \in \mathrm{W}_m \tag{26}$$

$$[\![v]\!] \cdot n = (\tau \cdot \nabla)\left\{r \cdot n \left[\!\left[V \cdot \tau\right]\!\right]\right\} + r \cdot n \left[\!\left[V \cdot \tau (\tau \cdot \nabla) \ell n \bar{\rho}\right]\!\right] = 0, \qquad x \in \mathrm{W}_m \tag{27}$$

where r is the complex amplitude of the wake displacement, the wake mean positions W_m are assumed to coincide with the mean-flow stagnation streamlines, and $\kappa = \tau \cdot \partial n/\partial \tau = -n \cdot \partial \tau/\partial \tau$ is the curvature of the mean wake surface. Equations (26) and (27) provide two independent relations for determining the jumps in the linearized unsteady pressure $[\![p]\!]$ and normal velocity component $[\![v]\!] \cdot n$ across each wake. However, since the wake normal displacement, $r \cdot n$, is also an unknown, these relations are not sufficient, unless the jumps in the steady tangential velocity and density are known across the wake.

Although not given explicitly here, the linearized equations that insure that mass, momentum, and energy are conserved to within first order across a shock are obtained by expanding the nonlinear time-dependent conditions, Eqs. (14–16), according to Eqs. (19–21), and performing the necessary algebra. The resulting expressions govern the jumps in the first-order fluid properties p, v, and s across moving shocks and the normal component of the shock displacement $r \cdot n$. Again, however, there is one more unknown associated with the unsteady jump conditions than independent equations. Since the surface conditions are not sufficient for fitting wakes and shocks into an unsteady solution based on the linearized Euler equations, additional information will be required.

We have assumed that the mean or steady flow at inlet ($\xi < \xi_-$) is at most a small irrotational perturbation from a uniform stream. By Kelvin's theorem, a similar condition will apply far downstream ($\xi > \xi_+$) if no strong shocks are present in the flow. Small steady or unsteady perturbations of a uniform freestream are governed by constant-coefficient field equations for which analytical solutions can be determined. In particular, it can be shown that a small-amplitude unsteady perturbation of a uniform mean flow can be decomposed into distinct entropic-, vortical-, and acoustic-type modes.[64,65] The entropic and vortical disturbances are convected without distortion by the uniform mean flow, and the vortical disturbance has a divergence-free velocity field. The acoustic disturbance is directly related to an irrotational velocity fluctuation, i.e., $p = -\bar{\rho}\bar{\mathrm{D}}\phi/\mathrm{D}t$, and its kinematical behavior is quite different from that of a vortical or entropic disturbance.

Each of the foregoing modes of unsteady motion, i.e.,

$$s(x) = s_{-\infty} \exp(i\kappa_{-\infty} \cdot x), \qquad \xi < \xi_- \tag{28}$$

$$\zeta(x) = \zeta_{-\infty} \exp(i\kappa_{-\infty} \cdot x), \qquad \xi < \xi_- \tag{29}$$

and

$$p_{I,\mp\infty}(x) = p_{I,\mp\infty} \exp(-\beta_{\mp\infty}\xi + i\kappa_{\mp\infty} \cdot x), \qquad \xi \lessgtr \xi_\mp \tag{30}$$

is a solution of the governing equations and can therefore be imposed on a uniform flow independently of the others. The circumferential wave number $\kappa_{\eta,\mp\infty}$ of a disturbance is σG^{-1}. The axial wave number $\kappa_{\xi,\mp\infty}$ of an entropic or vortical disturbance is determined by the relation $\omega = -\boldsymbol{\kappa}_{-\infty} \cdot \boldsymbol{V}_{-\infty}$. The attenuation constant $\beta_{\mp\infty}$ and axial wave number $\kappa_{\xi,\mp\infty}$ of an acoustic excitation also depend on the inlet/exit freestream velocity, the temporal frequency, and the circumferential wave number of the excitation, but via more complicated relationships.

Equations (28–30) indicate the far-field information that must be supplied to determine a linearized unsteady flow solution. In particular, the interblade phase angle σ, the temporal frequency ω, the complex amplitudes (at $x = 0$) of the entropic $s_{-\infty}$ and vortical $\zeta_{-\infty}$ excitations at inlet, and the pressure $p_{I,\mp\infty}$ excitations at inlet and exit must be prescribed. Usually only acoustic excitations that are of propagating type ($\beta_{\mp\infty} = 0$) are considered. Acoustic response disturbances that travel away from the blade row and entropic and vortical disturbances that are convected through the downstream boundary must be determined as part of the unsteady solution. It should be noted that if strong shocks are present in the inviscid flow, the far downstream steady velocity will not be uniform. An analytic solution for a pressure excitation from downstream [indicated by the subscript $+\infty$ in Eq. (30)] is not available in this case.

Isentropic and Irrotational Mean Flow

If any shocks that occur in the flow are, at most, of weak to moderate strength, then the steady background flow can be regarded as isentropic (with $S = 0$) and irrotational; i.e., $\boldsymbol{V} = \nabla\Phi$, where Φ is a steady velocity potential. In this case, the mass conservation equation for the underlying steady flow is

$$\nabla \cdot (\bar{\rho} \nabla \Phi) = 0 \tag{31}$$

and the momentum equation can be integrated to yield the following (Bernoulli) relations for the mean-flow variables:

$$(M_{-\infty}A)^2 = \bar{\rho}^{\gamma-1} = (\gamma M_{-\infty}^2 P)^{(\gamma-1)/\gamma}$$

$$= 1 - \frac{\gamma-1}{2} M_{-\infty}^2 \left[(\nabla\Phi)^2 - 1\right] \tag{32}$$

where M and A are the local steady Mach number and speed of sound propagation, respectively. The flow tangency condition, $\nabla\Phi \cdot \boldsymbol{n} = 0$, applies at the blade surfaces B_m, and the steady pressure and normal velocity component must be continuous across blade wakes W_m. Since entropy and vorticity changes across shocks $Sh_{m,n}$ are regarded as negligible, the mass, momentum, and energy conservation laws cannot all be enforced at such surfaces. The usual practice is to require only that mass and tangential momentum be conserved, i.e., $[\![\bar{\rho}\boldsymbol{V}]\!] \cdot \boldsymbol{n} = 0$ and $[\![\bar{\boldsymbol{V}}]\!] \cdot \boldsymbol{\tau} = 0$, respectively.

Numerical procedures for determining two-dimensional steady potential flows through cascades have been developed extensively, e.g., see Refs. 66 and 67, particularly for flows with subsonic relative inlet and exit Mach numbers (i.e., $M_{\mp\infty} < 1$). In such calculations a Kutta condition is usually imposed at blade trailing edges in lieu of prescribing an exit freestream flow property. Also, the usual practice is to solve the conservative form of the mass-balance equation, Eq. (31), throughout the entire fluid domain. Thus, shock-jump conditions are not imposed. Instead, as in nonlinear Euler calculations, shocks are captured through the use of special differencing techniques. In potential calculations the wake conditions are satisfied implicitly because the steady fluid properties are continuous and differentiable across wakes.

Unsteady Perturbation

As indicated by Goldstein,[65,68] the system of field equations that governs the linearized unsteady perturbation of a potential mean flow can be cast into a very convenient form by decomposing the unsteady velocity into rotational ($\boldsymbol{v}_R$) and irrotational ($\nabla\phi$) parts. The rotational velocity $\boldsymbol{v}_R$ is taken to be divergence free far upstream of the blade row, i.e., $\nabla \cdot \boldsymbol{v}_R \equiv 0$ for $\xi < \xi_-$, and the unsteady pressure depends only on the potential ϕ through the relation $p = -\bar{\rho}\bar{\mathrm{D}}\phi/\mathrm{D}t$. However, for realistic blade profiles, $\boldsymbol{v}_R \cdot \boldsymbol{n}$ and hence $\nabla\phi \cdot \boldsymbol{n}$ will be singular along the mean blade and wake surfaces. Therefore, Atassi and Grzedzinski[69] introduced a modified form of the Goldstein decomposition, i.e.,

$$\boldsymbol{v} = \boldsymbol{v}_* + \nabla\phi = \boldsymbol{v}_R + \nabla\phi_* + \nabla\phi \tag{33}$$

to facilitate the numerical resolution of the velocity potential ϕ. Here, ϕ_* is a convected or pressureless potential (i.e., $\bar{\mathrm{D}}\phi_*/\mathrm{D}t = 0$) that satisfies the condition $\nabla\phi_* \cdot \boldsymbol{n} = -\boldsymbol{v}_R \cdot \boldsymbol{n}$ at blade and wake mean positions.

The system of field equations that governs the linearized unsteady flow variables s, $\boldsymbol{v}_R$, and ϕ is determined by substituting the velocity decomposition, Eq. (33), into the linearized Euler equations, Eqs. (22–24), to obtain

$$\frac{\bar{\mathrm{D}}s}{\mathrm{D}t} = 0 \tag{34}$$

$$\frac{\bar{\mathrm{D}}}{\mathrm{D}t}\left(\boldsymbol{v}_R - \frac{s\nabla\Phi}{2}\right) + \left[\left(\boldsymbol{v}_R - \frac{s\nabla\Phi}{2}\right) \cdot \nabla\right] \nabla\Phi = 0 \tag{35}$$

and

$$\frac{\bar{\mathrm{D}}}{\mathrm{D}t}\left(A^{-2}\frac{\bar{\mathrm{D}}\phi}{\mathrm{D}t}\right) - \bar{\rho}^{-1}\nabla \cdot (\bar{\rho}\nabla\phi) = \bar{\rho}^{-1}\nabla \cdot (\bar{\rho}\boldsymbol{v}_*) \tag{36}$$

These equations are coupled only sequentially; hence, they can be solved in succession to determine the complex amplitudes of the entropy s, rotational velocity $\boldsymbol{v}_R$, and velocity potential ϕ, respectively. Moreover, closed-form solutions[30,65] can be determined for the entropy and rotational velocity fluctuations in terms of the known conditions at inlet. The velocity potential ϕ is governed by a second-order partial differential equation, along with conditions at the blade, wake, and shock surfaces and at the inlet and exit boundaries, and must be determined using numerical field methods.

Entropy and Rotational Velocity

We introduce the Lagrangian independent variable, $\boldsymbol{X} = \Delta\boldsymbol{e}_T + \Psi\boldsymbol{e}_N$, where

$$\Delta(\boldsymbol{x}) = \boldsymbol{x}_- \cdot \boldsymbol{e}_T + \int_{x_- + [\Psi(x) - \Psi(x_-)]\boldsymbol{e}_N}^{x} V^{-1}\, \mathrm{d}\tau_\Psi$$

$$\Psi(\boldsymbol{x}) = \boldsymbol{x}_- \cdot \boldsymbol{e}_N + \int_{x_-}^{x} \bar{\rho}(\boldsymbol{e}_z \times \boldsymbol{V}) \cdot \mathrm{d}\boldsymbol{\tau} \tag{37}$$

are the drift and stream functions, respectively, of the steady background flow. The unit vectors $\boldsymbol{e}_T$, $\boldsymbol{e}_N (= \boldsymbol{e}_z \times \boldsymbol{e}_T)$ and $\boldsymbol{e}_z$ point in the inlet freestream direction, normal to the inlet freestream direction, and out from the page, respectively; $\boldsymbol{x}_-$ is the position vector to the point of intersection (ξ_-, η_-) of the reference blade ($m = 0$) stagnation streamline and the axial line $\xi = \xi_-$; $\mathrm{d}\tau_\Psi$ is a differential element of arc length along a streamline; and $\mathrm{d}\boldsymbol{\tau}$ is a differential vector tangent to the path of integration.

The solutions to the entropy, Eq. (34), and rotational velocity, Eq. (35), transport equations can be expressed in the form[65]

$$s(\boldsymbol{x}) = s_{-\infty} \exp(i\boldsymbol{\kappa}_{-\infty} \cdot \boldsymbol{X}) \tag{38}$$

and

$$\boldsymbol{v}_R(\boldsymbol{x}) = \left[\nabla(\boldsymbol{X} \cdot \boldsymbol{\mathfrak{A}}_{-\infty}) + s_{-\infty}\nabla\Phi/2\right] \exp(i\boldsymbol{\kappa}_{-\infty} \cdot \boldsymbol{X}) \tag{39}$$

where $\boldsymbol{\mathfrak{A}}_{-\infty} = \boldsymbol{v}_{R,-\infty} - s_{-\infty}\boldsymbol{V}_{-\infty}/2$. Since $\zeta_{-\infty} = i\boldsymbol{\kappa}_{-\infty} \times \boldsymbol{v}_{R,-\infty}$ and the rotational velocity is divergence free far upstream of

the blade row, the vectors $\kappa_{-\infty}$ and $v_{R,-\infty}$ are orthogonal and $v_{R,-\infty} = i(\kappa_{-\infty} \times \zeta_{-\infty})/|\kappa_{-\infty}|^2$.

For realistic configurations the steady background flow stagnates at blade leading edges. Therefore, the drift function has a logarithmic singularity, i.e., $\Delta \to a_0 \ell n$, at the mean blade and wake surfaces, and the rotational velocity is singular at such surfaces. A convected potential of the form[69]

$$\phi_*(x) = \left[-i\omega^{-1}\mathfrak{A}_{-\infty} \cdot V_{-\infty} + F(\Psi)\right] \exp(i\kappa_{-\infty} \cdot X) \tag{40}$$

where

$$F(\Psi) = \frac{\omega^{-1} G \cos \Omega_{-\infty} (\kappa_{-\infty} \times \mathfrak{A}_{-\infty}) \cdot e_z}{2\pi(1 - ia_0\omega)} \sin\left\{\frac{2\pi[\Psi(x) - \Psi(x_-)]}{G \cos \Omega_{-\infty}}\right\} \tag{41}$$

insures that $v_* \cdot n = (v_R + \nabla\phi_*) \cdot n = 0$ at the mean blade and wake surfaces and, hence, that $\nabla\phi \cdot n$ is finite at such surfaces.

The unsteady flow variables s, v_R, and ϕ_* can be evaluated once the drift and stream functions of the steady background are determined. The unsteady potential ϕ can then be found numerically as a solution of the field equation (36) subject to the appropriate surface and far-field conditions. The flow tangency condition (25) with $V = \nabla\Phi$ and $v \cdot n = \nabla\phi \cdot n$ applies at the mean blade surfaces B_m. Since the irrotational steady velocity and density are continuous downstream of the blade row, the linearized unsteady pressure and normal velocity component are continuous across the mean wakes W_m, i.e., $[\![D\phi/Dt]\!] = 0$ and $[\![\nabla\phi]\!] \cdot n = 0$. Finally, if we neglect changes in entropy $[\![s]\!]$ and vorticity $[\![\zeta]\!]$ across shocks and combine the conservation laws for mass and tangential momentum, we obtain the following condition for determining the jump in ϕ across a shock ($x \in \mathrm{Sh}_{m,n}$) that terminates in the fluid:

$$\left[\!\!\left[\bar{\rho}\left(\nabla\phi + v_* - A^{-2}\frac{D\phi}{Dt}\nabla\Phi\right)\right]\!\!\right] \cdot n = [\![\bar{\rho}]\!]\left[i\omega + (\nabla\Phi \cdot \tau)\tau \cdot \nabla\right](r \cdot n) + (r \cdot n)\tau \cdot \nabla\left([\![\bar{\rho}]\!]\nabla\Phi \cdot \tau\right) \tag{42}$$

where $r \cdot n = -([\![\nabla\Phi]\!] \cdot n)^{-1}[\![\phi]\!]$ is the shock displacement normal to the mean shock locus. The velocity potential fluctuations in the far upstream and far downstream regions depend on the prescribed acoustic excitation as well as the acoustic and vortical response of the cascade. We can set $\phi(x) = \phi_E(x) + \phi_R(x)$ for $\xi \lessgtr \xi_{i,\mp}$, where ϕ_E accounts for acoustic excitations and is therefore prescribed, and ϕ_R is associated with the response of the blade row and therefore must be determined as part of the unsteady solution. Analytic solutions for ϕ_R can be determined[63] that satisfy the requirements that acoustic response disturbances either attenuate with increasing axial distance from the blade row or propagate carrying energy away from or parallel to the blade row and that vorticity must be convected downstream. These solutions can be matched to a near-field numerical solution to close the boundary-value problem for the unsteady potential.

Aeroelastic Response Parameters

Solutions to the foregoing nonlinear steady and linearized unsteady flow problems are required to determine the aerodynamic response information needed for blade-row aeroacoustic and aeroelastic predictions, i.e., the unsteady pressure response at inlet and exit and the unsteady pressures acting at the moving blade surfaces. We will proceed to describe the local and global unsteady aerodynamic response parameters that are used in linear aeroelastic investigations, but refer the reader to Ref. 70 for more detailed information.

The pressure acting at the instantaneous position of the reference ($m = 0$) blade surface is given by

$$\tilde{P}(\tau_{\mathfrak{B}}, t) = P(\tau_{\mathrm{B}}) + \tilde{p}_{\mathfrak{B}}(\tau_{\mathrm{B}}, t) + \sum_n \tilde{P}_{\mathrm{Sh}_n}(\tau_{\mathrm{B}}, t) + \cdots \tag{43}$$

where $\tilde{p}_{\mathfrak{B}} = \mathrm{Re}\{p_{\mathfrak{B}} \exp(i\omega t)\}$, $p_{\mathfrak{B}} = [p + (r \cdot \nabla)P]_{\mathrm{B}}$, τ measures distance in the counterclockwise direction along the blade surface, and the subscripts $\mathfrak{B}$ and B refer to the instantaneous and mean blade surfaces, respectively. The first two terms on the right-hand side of Eq. (43) are the steady and the first-harmonic unsteady pressures acting at the moving blade surface. The third term is the anharmonic unsteady pressure associated with shock motion and is determined by analytically continuing the steady and the first-harmonic unsteady solutions from the mean to the instantaneous shock locations.[71] Although the unsteady pressure response is not everywhere harmonic, its integral over a blade surface and, consequently, the first-order global unsteady aerodynamic loads are harmonic in time.[72]

For aeroelastic calculations, it is convenient to introduce a set of generalized forces corresponding to a set of independent, but otherwise arbitrary, structural deformation modes. For this purpose, the reference blade displacement can be expressed in the form

$$\mathfrak{R}_B(x, t) = \sum_{i=1}^{I} \tilde{\delta}_i(t) R_i(x) = \sum_{i=1}^{I} \mathrm{Re}\left[\delta_i \exp(i\omega t)\right] R_i(x) = \mathrm{Re}\left[r_B(x) \exp(i\omega t)\right] \tag{44}$$

where the generalized coordinate $\tilde{\delta}_i(t)$ describes the amplitude of the motion in the ith mode, $R_i(x)$ is a real vector function that describes the shape and direction of this displacement, and we have used the subscript B to indicate blade displacement. The ith generalized force is then defined as

$$\tilde{Q}_i(t) = -\oint_{\mathfrak{B}} \tilde{P} n \cdot R_i \, d\tau = Q_i + \tilde{q}_i + \cdots \tag{45}$$

where the unit normal vector n points out from the blade surface, and Q_i and $\tilde{q}_i = \mathrm{Re}[q_i \exp(i\omega t)]$ are the steady and the first-harmonic unsteady components, respectively, of the time-dependent generalized force $\tilde{Q}_i(t)$. After replacing the surface integration in Eq. (45) by an integration over the mean blade surface and performing some algebra,[70] we find that

$$q_i = \oint_B q_{i,\tau} \, d\tau = -\oint_B \left[P \frac{\partial r_B}{\partial \tau} \times e_z + p_{\mathfrak{B}} n - \sum_n r_{\mathrm{Sh}_n,B} [\![P]\!]_{\mathrm{Sh}_n} \delta(\tau - \tau_{\mathrm{Sh}_n}) n\right] \cdot R_i \, d\tau \tag{46}$$

where $q_{i,\tau}$ is the distributed ith generalized force, $r_{\mathrm{Sh}_n,B} = (r_{\mathrm{Sh}_n} - r_B) \cdot \tau_B$ is the complex amplitude of the relative shock displacement along the moving blade surface, $\delta(\tau)$ is the Dirac delta function, and the subscript Sh_n refers to the mean nth shock location.

Two time-independent, real parameters that are also useful in describing the aerodynamic response to prescribed blade vibrations are the work per cycle W_C and the pressure displacement function $w(\tau)$. The former is the work done by an airstream on a given blade over one cycle of its motion. Therefore, a prescribed blade motion is stable, neutrally stable, or unstable according to whether the work per cycle is less than, equal to, or greater than zero, respectively. The pressure-displacement function describes the distribution of the work per cycle over a blade surface. If the blade motion is expressed in terms of generalized coordinates, as in Eq. (44), then

$$W_C = \oint_B w(\tau) \, d\tau = \pi \oint_B \mathrm{Im}\left(\sum_{i=1}^{I} \delta_i^* q_{i,\tau}\right) d\tau = \pi \mathrm{Im}\left(\sum_{i=1}^{I} \delta_i^* q_i\right) \tag{47}$$

where the superscript * denotes the complex conjugate.

An important special case for turbomachinery aeroelastic calculations is one in which each incremental two-dimensional blade section vibrates in a rigid-body mode consisting of a translation in the y direction and a counterclockwise rotation

about an axis at $x = x_P$. In this case, $r_B = \delta_1 e_y + \delta_2(e_z \times R_P)$, where the vector R_P extends from the mean position of the reference blade axis of rotation x_P to a point on the mean reference blade surface. The generalized forces $\tilde{q}_1$ and $\tilde{q}_2$ represent, therefore, the first-harmonic unsteady aerodynamic lift and moment about the fixed axis at $x = x_P$. We find that $q_1 = f \cdot e_y$, $q_2 = m_\Phi + \delta_2 M_P$, and $W_C = \pi \mathrm{Im}(\delta_1^* f \cdot e_y + \delta_2^* m_\Phi)$, where $f \cdot e_y$ and m_Φ are the complex amplitudes of the first-harmonic unsteady aerodynamic lift and moment about the moving pitching axis at $x = x_\Phi$, respectively, and M_P is the zeroth-order or steady moment about the mean pitching axis at $x = x_P$.

Linearized Solution Methods

Numerical procedures for calculating unsteady perturbations of isentropic and irrotational steady background flows have received a great deal of attention. Recent developments include the prediction of discontinuous unsteady transonic flows excited by blade vibrations[29] and the prediction of the unsteady subsonic flows excited by vortical gusts.[30,31] Potential-based linearizations are very efficient, requiring only about 10 CPU s on a Cray YMP. At present, work is proceeding to apply such analyses in blade row aeroelastic[73,74] and aeroacoustic[75] studies and to couple linearized inviscid analyses to unsteady viscous-layer analyses to provide weak and strong inviscid/viscid interaction (IVI) solution capabilities for unsteady cascade flows.[76,77]

Two potential-based unsteady aerodynamic linearizations called FINSUP and LINFLO have received wide application. The FINSUP analysis[22,25,27,67] applies at subsonic and supersonic inlet and exit Mach numbers and to unsteady flows excited by prescribed blade motions and acoustic excitations at inlet and exit. Here, the nonlinear steady and the first harmonic unsteady equations are approximated on a fixed, unstructured, triangular mesh using a finite element spatial discretization. Shock effects are captured in both the nonlinear steady and the linearized unsteady analyses. The steady equations are solved using a Newton iteration procedure in which each member of a sequence of approximations to the nonlinear steady solution are determined by direct matrix inversion via Gaussian elimination. The complex linear unsteady equations are solved directly using a similar inversion procedure.

The LINFLO analysis[26,28-30] applies at subsonic inlet and exit Mach numbers and to unsteady cascade flows excited by prescribed blade motions, entropic and vortical excitations at inlet, and acoustic excitations at inlet and exit. LINFLO treats only the linearized unsteady flow problem; therefore, steady background flow information must be supplied as input for an unsteady flow calculation. For the most part, the cascade, full-potential analysis of Caspar[66] has been used for this purpose. The linearized unsteady equations are discretized, using an implicit, least-squares, finite difference approximation[78] on a fixed composite mesh,[29] consisting of a blade-passage H mesh and a local C mesh that wraps around a blade. Although the H mesh alone is usually sufficient for resolving subsonic flows, the local mesh allows an accurate modeling of leading-edge and shock phenomena. Shocks are captured in the steady analysis but fitted in the linearized unsteady calculation via the implementation of the shock-jump condition, Eq. (42).

A linearized Euler analysis was first proposed by Ni and Sisto[79] so that strong shock effects could be taken into acount in unsteady flow calculations. However, because of the associated computing requirements, significant progress has been achieved only recently. In particular, Hall and Crawley[32] approximated the conservative forms of the nonlinear steady and the first-harmonic unsteady Euler equations on a fixed H grid using a finite volume discretization. The steady equations are solved via Newton iteration. Successive approximations to the final steady solution, as well as a direct linearized unsteady flow solution, are obtained by applying Gaussian elimination to a large sparse system of linear algebraic equations. Results, determined by shock fitting, for a two-dimensional unsteady flow through a hyperbolic channel show an excellent definition of unsteady shock phenomena. In particular, the calculated moving shock remains normal to the channel walls at all times, and the amplitude of the shock displacement varies along the shock, decreasing with increasing shock strength.

Because of the difficulties anticipated in implementing a direct solution procedure for three-dimensional flows and in fitting shocks and wakes in complicated two- and three-dimensional unsteady cascade flows, Hall and Clark[33] have recently proposed a time-marching Euler procedure for steady and linearized unsteady flows. Here, the conservative forms of the nonlinear steady and first-harmonic unsteady Euler equations are solved by advancing solutions in pseudotime to steady and periodic unsteady states, respectively, using Ni's[80] Lax-Wendroff technique. Shocks and wakes are captured in both the steady and the unsteady flow calculations. The linearized unsteady equations are solved on a harmonically deforming H grid, thereby avoiding the need to approximate the mean-flow gradient terms [i.e., $(r \cdot \nabla)V$ in Eq. (25) and $r \cdot \nabla P$, see Eq. (43)] that arise from transferring surface information from the instantaneous to the mean surface locations. The method requires approximately 1 CPU min of time on a Cray YMP for a representative, two-dimensional, subsonic calculation. Results for subsonic flat-plate and compressor cascades are in very good agreement with those of classical and full-potential based unsteady aerodynamic linearizations, respectively.

Example Response Predictions

Theoretical results will be presented to indicate the status of linearized unsteady aerodynamic prediction methods and to demonstrate several important features associated with the aerodynamic response of isolated two-dimensional blade rows to prescribed blade vibrations and vortical disturbances at inlet. We consider two compressor-type cascades, both operating at subsonic inlet conditions. The first, a high-speed compressor cascade, consists of cambered NACA 0006 airfoils and operates at an inlet Mach number of 0.8; the second, a compressor exit guide vane (EGV), consists of highly cambered NACA 0012 blades and operates at an inlet Mach number of 0.3.

These configurations can serve as useful benchmarks for evaluating various unsteady aerodynamic prediction methods. Indeed, the NACA 0006 cascade has been designated as one of the standard cascade configurations[81] for establishing a theoretical and experimental data base for unsteady cascade flows. Consequently, a number of investigators have applied linearized analyses, both potential based and Euler, and time-marching Euler and Navier-Stokes simulations to this configuration. Thus far, the result comparisons have been encouraging. In particular, Huff[82] has applied a nonlinear Euler analysis to several of the transonic cases reported herein and has found very good agreement between his nonlinear and the linearized response predictions.

Here, the steady background flows are assumed to be isentropic and irrotational and to satisfy a Kutta condition at blade trailing edges. Therefore, only information on the inlet freestream conditions, e.g., inlet Mach number and flow angle, is required to calculate the steady flowfields. The linearized unsteady flows through the NACA 0006 cascade are excited by prescribed single-degree-of-freedom (SDOF) blade motions at unit amplitude, ($|\delta_i| = 1$); those through the EGV, by prescribed vortical gusts with $v_{R,-\infty} \cdot e_N = (1, 0)$. These unsteady excitations are termed subresonant if all acoustic response waves attenuate with increasing axial distance from the blade row and superresonant (m, n) if m and n such waves persist far upstream and/or far downstream, respectively, and carry energy away from the blade row. An acoustic resonance occurs if at least one wave persists in the far field and carries energy along the blade row.

Theoretical results, including steady Mach number distributions and global and local unsteady aerodynamic response predictions, are presented in Figs. 7-12. The steady-flow pre-

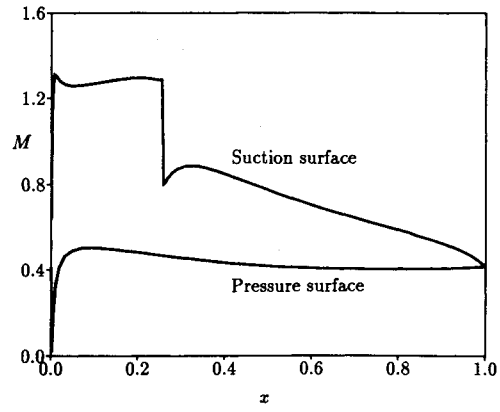

Fig. 7 Surface Mach number distributions for the transonic NACA 0006 cascade: $M_{-\infty}=0.8$, $\Omega_{-\infty}=58$ deg.

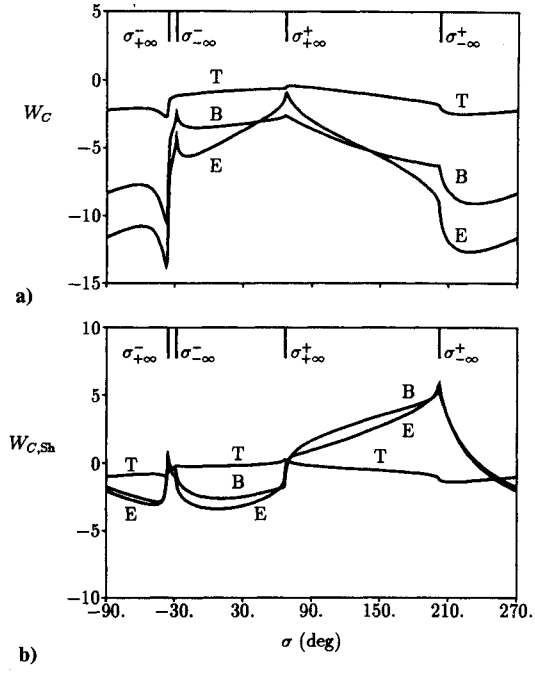

Fig. 8 Work per cycle vs interblade phase angle for unit frequency, SDOF motions of the transonic NACA 0006 cascade: B, E, and T denote bending, chordwise bending (elastic), and torsional blade motions, respectively; a) work per cycle, b) work per cycle due to shock motion.

dictions have been determined using the cascade full potential analysis of Ref. 66; the unsteady results, using the LINFLO analysis. The unsteady transonic solutions for the NACA 0006 cascade have been determined on a composite (H/C) mesh. Subsonic solutions for the EGV and a corresponding flat-plate cascade have been determined using an H mesh alone. More extensive results for the NACA 0006 and the EGV configurations can be found in Refs. 29, 30, 70, and 77.

Transonic NACA 0006 Cascade

This cascade has a stagger angle Θ of 45 deg and a gap/chord ratio G of unity and operates at an inlet Mach number $M_{-\infty}$ of 0.8 and flow angle $\Omega_{-\infty}$ of 58 deg. The blades are constructed by superposing the thickness distribution of a NACA 0006 airfoil on a circular-arc camber line having a height at blade midchord of $y=0.05$.[70] The mean or steady flow through the cascade is transonic with a single normal shock occurring in each blade passage. The predicted blade-surface Mach number distributions are shown in Fig. 7. The transonic mean flow stagnates on the pressure surface at $x=0.002$, and the normal shock impinges on the suction surface at $x=0.257$. The Mach numbers at the base of the shock are 1.292 on the upstream side and 0.794 on the downstream side, and the exit Mach number and flow angle are 0.432 and 40.3 deg, respectively. The mean lift force acting on each blade is 0.412, and the jump in the steady pressure at the base of the shock, $[\![P_B]\!]$, is -0.494.

Work per cycle predictions are given in Fig. 8 for pure bending ($\boldsymbol{R}=\boldsymbol{e}_y$), pure torsional ($\boldsymbol{R}=\boldsymbol{e}_z\times\boldsymbol{R}_P$) about midchord ($x_P=0.5, 0$), and pure chordwise bending or elastic ($\boldsymbol{R}=\boldsymbol{e}_y \sin \pi x$) modes of blade vibration at unit amplitude $|\delta_i|=1$ and unit frequency $\omega=1$. The vertical lines above the curves denote the resonant interblade phase angles for a unit-frequency excitation. The curves in Fig. 8a indicate that the SDOF bending, torsional, and chordwise bending motions at unit frequency are stable ($W_C<0$) and that the torsional vibrations have the lowest stability margin. They also indicate the rather complicated nature of the global unsteady aerodynamic response associated with realistic cascade flows, which results from the different acoustic responses [i.e., subresonant, super resonant (1,0), etc.] produced by unit-frequency excitations at different interblade phase angles. Note that abrupt changes in global unsteady aerodynamic response behavior appear at the interblade phase angles at which an acoustic resonance occurs.

As noted previously, there are two contributions to the unsteady airloads for a discontinuous transonic flow: one arising from the first harmonic unsteady pressure response and the other arising from the anharmonic pressure response associated with shock motion. Shock-induced work per cycle responses, i.e., $W_{C,Sh}=\mathrm{Im}\{r_{Sh,B}([\![P_B]\!]\,\boldsymbol{n}_B\cdot\boldsymbol{r}^*_B)_{Sh}\}$, for the transonic NACA 0006 cascade are shown in Fig. 8b. These results indicate that the shock loads tend to support the unit-frequency bending and chordwise bending motions over a broad range of interblade phase angles, i.e., 70 deg $\lesssim\sigma\lesssim$ 240 deg. Also, these loads become quite severe for interblade phase angles near the upstream resonance condition, $\sigma=\sigma^+_{-\infty}$. The

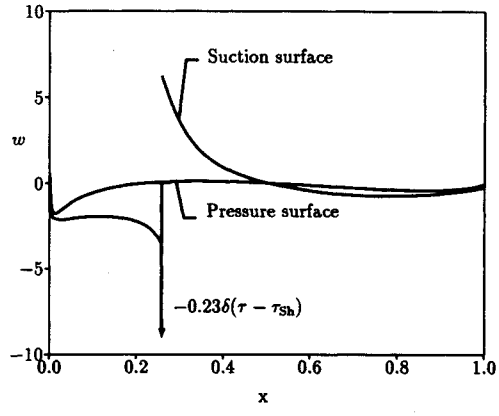

Fig. 9 Pressure-displacement function distribution for the transonic NACA 0006 cascade due to an in-phase torsional vibration about midchord at $\omega=1.0$.

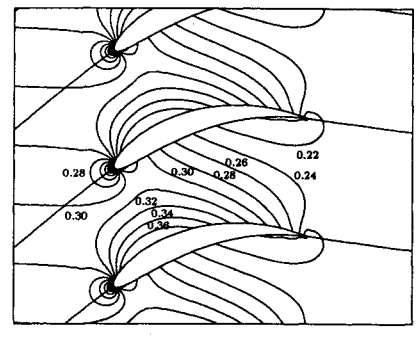

Fig. 10 Mach number contours for steady flow at $M_{-\infty}=0.3$ and $\Omega_{-\infty}=40$ deg through the EGV cascade.

pure torsional motions at $\omega = 1$ give rise to relatively smaller shock loads, and these usually act to resist or stabilize the blade motions.

A benefit of using the work per cycle to describe global unsteady aerodynamic response behavior is that the responses to different modes of blade motion, including coupled modes, can be represented via this single, real, global response parameter. The pressure displacement or local work per cycle function serves the same purpose for describing the local response. A pressure displacement function distribution for the transonic NACA 0006 cascade is shown in Fig. 9 for a case in which the blades undergo a unit-amplitude, in-phase ($\sigma = 0$ deg), torsional motion about midchord at $\omega = 1.0$. The work per cycle W_C for this in-phase motion is -0.92, and that due to the concentrated shock load $W_{C,Sh}$, indicated by the arrow in Fig. 9, is -0.23. Thus, the blade motion is stable, and the shock load contributes significantly to the stability margin. The first-harmonic, local, unsteady loads just downstream of the shock act to enhance or destabilize the in-phase torsional blade motion, but over most of the blade surface these local unsteady airloads suppress the motion.

Compressor Exit Guide Vane

The EGV has a stagger angle Θ of 15 deg and a blade spacing G of 0.6 and operates at a prescribed inlet Mach number $M_{-\infty}$ of 0.3 and inlet flow angle $\Omega_{-\infty}$ of 40 deg. The blades are constructed by superposing the thickness distribution of a NACA 0012 airfoil on a circular-arc camber line having a height at midchord of $y = 0.13$. The calculated steady Mach number contours for this configuration are shown in Fig. 10. The exit Mach number and exit flow angle are 0.226 and -7.4 deg, respectively, and the mean lift force acting on each blade is 0.36.

We consider unsteady flows that are excited by inlet vortical disturbances, and we examine the behavior of the unsteady vorticity and pressure fields that result from the interaction between the EGV and a vortical gust defined by $v_{R,-\infty} \cdot e_N = (1, 0)$, $\omega = 5$, and $\sigma = -2\pi$. In addition, we will examine the unsteady moment responses of the EGV and a corresponding flat-plate cascade (i.e., $\Theta = \Omega = 40$ deg, $G = 0.6$, and $M = 0.3$)

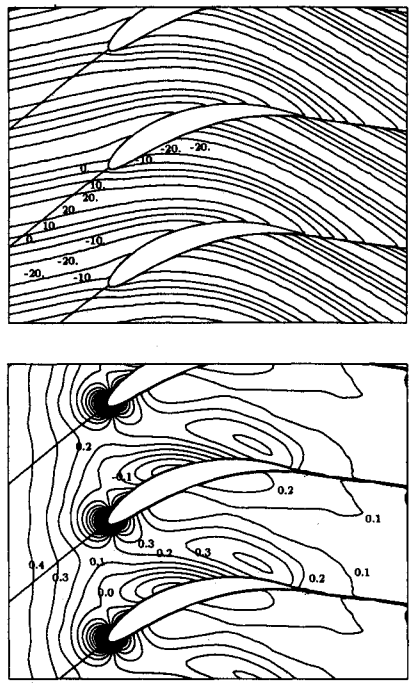

Fig. 11 Contours of the in-phase components (real parts) of the unsteady vorticity and the unsteady pressure for the EGV cascade subjected to an incident vortical gust with $v_{R,-\infty} \cdot e_N = (1, 0)$, $\omega = 5$, and $\sigma = -2\pi$.

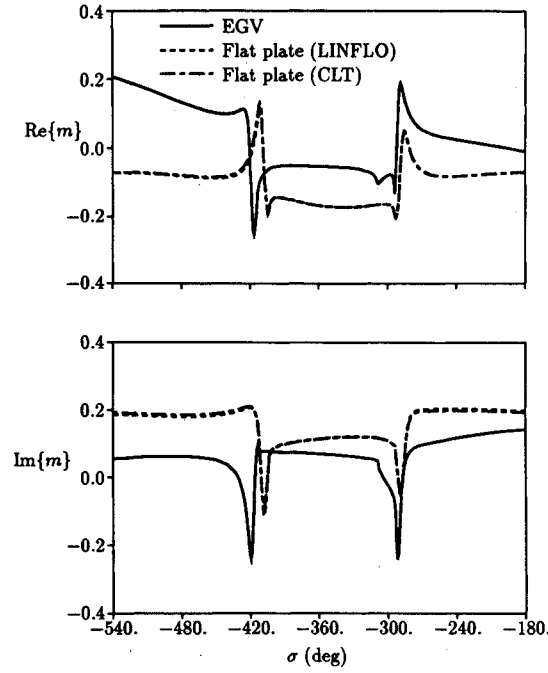

Fig. 12 Unsteady moment about midchord vs interblade phase angle for the EGV and corresponding flat-plate cascades subjected to vortical gusts with $v_{R,-\infty} \cdot e_N = (1, 0)$, and $\omega = 5$.

to vortical excitations at $v_{R,-\infty} \cdot e_N = (1, 0)$, $\omega = 5$, and $-3\pi \leq \sigma \leq -\pi$. Note that the unsteady moments are taken about midchord ($x_P = 0.5$, 0), and the mean positions of the flat-plate blades are aligned with the inlet freestream flow direction.

Contours of the real parts of the complex amplitudes of the unsteady vorticity $\mathrm{Re}\{\zeta\} = \mathrm{Re}\{\zeta\} e_z$ and the unsteady pressure $\mathrm{Re}\{p\}$ for the EGV are shown in Fig. 11. As indicated, the vortical gust is distorted as it is convected by the nonuniform mean flow through the EGV blade row. The mean flow stagnates in the vicinity of the blade leading edges, and consequently the vortex lines are severely stretched through thin regions adjacent to the mean blade and wake surfaces. In addition, since the vorticity is convected at different mean velocities along the upper and lower surfaces of the EGV blades, an observer moving across the wake of an EGV blade would encounter strong and abrupt changes in vorticity. The unsteady pressure field that arises from the interaction of this vortical gust with the EGV blade row is depicted at the bottom of Fig. 11. This pressure response is superresonant (1,1). A relatively strong acoustic response wave persists far upstream and carries energy away from the blade row; a very weak wave persists far downstream.

The unsteady moments (m) that act on the reference blades of the EGV and the corresponding flat-plate cascade are plotted vs interblade phase angle in Fig. 12 for vortical excitations at $v_{R,-\infty} \cdot e_N = (1, 0)$, $\omega = 5$, and -3π (-540 deg) $\leq \sigma \leq -\pi$ (-180 deg). Here, the excitations at $\sigma = -404.2$ and -293.9 deg produce resonant acoustic response disturbances far upstream and far downstream of the flat-plate blade row and far upstream of the EGV; those at $\sigma = -414.3$ and -308.8 deg produce such responses far downstream of the EGV. The vortical gusts are convected without distortion by the uniform mean flow through the flat-plate blade row, i.e., the rectilinear vorticity contour patterns that exist far upstream of the EGV persist throughout the flat-plate flowfield. The results in Fig. 12 indicate that gust distortions, due to mean-flow nonuniformities, have a substantial impact on the unsteady moment responses to vortical excitations. Note that the LINFLO and classical linear theory (CLT)[6] moment predictions for the flat-plate cascade are in excellent agreement.

Concluding Remarks

Two distinct approaches are being actively pursued to provide more accurate unsteady aerodynamic response information for turbomachinery aeroelastic and aeroacoustic design applications. In one, the time-dependent, nonlinear equations that describe viscid (i.e., the Reynolds-averaged Navier-Stokes equations) or inviscid (the Euler equations) fluid motion are solved by advancing numerical calculations in time until a converged periodic unsteady state is determined. In the other or more traditional approach, inviscid ($Re \rightarrow \infty$) and small unsteady disturbance assumptions are invoked to obtain time-independent, nonlinear, steady and linearized, unsteady equations that are solved sequentially to determine the steady and first-harmonic, unsteady inviscid flow properties. A very encouraging sign, at present, is that good agreement is being achieved between the results of the nonlinear, time-marching and the linearized frequency domain analyses for inviscid unsteady cascade flows driven by small-amplitude excitations.

An extensive effort has been under way to establish theoretical and experimental data bases on unsteady flows through selected two-dimensional cascades. The latter are referred to as the standard cascade configurations.[81,83,84] The goals of this effort are to provide convenient means for evaluating and comparing the results of different theoretical analyses and for assessing theoretical predictions through comparisons with experimental measurements. At present the theoretical results for a number of the standard configurations seem to be coming together; however, substantial agreement between analysis and experiment has been achieved only for the low-speed, low-frequency, unsteady flows through a vibrating, compressor blade row, studied experimentally by Carta.[85] Major difficulties must still be overcome to construct useful experiments and to provide benchmark data for the high-speed, high-frequency unsteady flows of practical interest. Thus, in the near term, theoretical procedures, founded on very limited experimental confirmation, will have to be relied on to provide the unsteady aerodynamic response information needed for aeroelastic and aeroacoustic design applications.

The computational requirements associated with time-accurate numerical simulations of nonlinear unsteady flows will continue to prohibit their implementation in aeroelastic or aeroacoustic design prediction systems. Thus, traditional methods must still be developed so that useful aerodynamic response information can be provided. Inviscid unsteady aerodynamic linearizations offer great promise for meeting the needs of designers for efficient solutions that contain much of the essential physics of practical unsteady cascade flows. However, methods must be developed to account for viscous displacement effects within a framework that includes a linearized inviscid analysis. A linearization of the viscous equations of motion may not be suitable for this purpose. If not, it will be necessary to couple linearized inviscid and nonlinear viscous-layer analyses, using an appropriate interaction law, to provide a useful inviscid/viscid interaction analysis for unsteady cascade flows. The traditional approach must also be extended for application to three-dimensional unsteady flows. Since strong shock phenomena do not usually play a critical role, a potential-based linearization is probably adequate for two-dimensional applications. However, since vortical effects associated with swirling mean flows are expected to be important, the linearized Euler approach is the natural one to consider for future extension to three-dimensional flows.

The major disadvantages of linearized inviscid and high Reynolds number inviscid/viscid interaction analyses are that they will have limited ranges of application, and they are difficult to develop. Thus, research to provide time-accurate numerical solutions for fully nonlinear unsteady flows must also continue. In the near term, this work should be directed towards providing a reliable "numerical test facility" for unsteady cascade flows. This facility could be used to determine the relative importance of the nonlinear effects associated with shock behavior, viscous separation, finite amplitude excitation, etc. It could also be used to indicate the regions of validity of approximate analyses and to provide unsteady aerodynamic response information in parametric regions in which the approximate methods fail.

Acknowledgments

Preparation of this article was supported under the United Technologies Corporate Research Program. The author would like to thank R. Rudewicz for her help in this effort. An earlier version of this paper was presented at the Sixth International Symposium on Unsteady Aerodynamics, Acoustics, and Aeroelasticity of Turbomachines and Propellers held at the University of Notre Dame, Notre Dame, Indiana, in September 1991.

References

[1]Mikolajczak, A. A., Arnoldi, R. A., Snyder, L. E., and Stargardter, H., "Advances in Fan and Compressor Blade Flutter Analysis and Predictions," *Journal of Aircraft,* Vol. 12, No. 4, 1975, pp. 325–332.

[2]Fleeter, S., "Aeroelasticity Research for Turbomachine Applications," *Journal of Aircraft,* Vol. 16, No. 5, 1979, pp. 320–326.

[3]Fleeter, S., and Jay, R. L., "Unsteady Aerodynamic Measurements in Flutter Research," *AGARD Manual on Aeroelasticity in Axial-Flow Turbomachines, Unsteady Turbomachinery Aerodynamics,* Vol. 1, edited by M. F. Platzer and F. O. Carta, AGARD-AG-298, March 1987, Chap. VIII.

[4]Groeneweg, J. F., and Rice, E. J., "Aircraft Turbofan Noise," *Transactions of the American Society of Mechanical Engineers: Journal of Turbomachinery,* Vol. 109, No. 1, 1987, pp. 130–141.

[5]Whitehead, D. S., "Classical Two-Dimensional Methods," *AGARD Manual on Aeroelasticity in Axial-Flow Turbomachines, Unsteady Turbomachinery Aerodynamics,* Vol. 1, edited by M. F. Platzer and F. O. Carta, AGARD-AG-298, March 1987, Chap. III.

[6]Smith, S. N., "Discrete Frequency Sound Generation in Axial Flow Turbomachines," British Aeronautical Research Council, R&M 3709, London, March 1972.

[7]Whitehead, D. S., "Vibration and Sound Generation in a Cascade of Flat Plates in Subsonic Flow," British Aeronautical Research Council, R&M 3685, London, Feb. 1970.

[8]Kaji, S., and Okazaki, T., "Propagation of Sound Waves Through a Blade Row, II: Analysis Based on the Acceleration Potential Method," *Journal of Sound and Vibration,* Vol. 11, No. 3, 1970, pp. 355–375.

[9]Surampudi, S. P., and Adamczyk, J. J., "Unsteady Transonic Flow over Cascade Blades," *AIAA Journal,* Vol. 24, No. 2, 1986, pp. 293–302.

[10]Verdon, J. M., "Further Developments in the Aerodynamic Analysis of Unsteady Supersonic Cascades, I: The Unsteady Pressure Field, II: Aerodynamic Response Predictions," *Transactions of the American Society of Mechanical Engineers: Journal of Engineering for Power,* Vol. 99, No. 4, 1977, pp. 509–525.

[11]Nagashima, T., and Whitehead, D. S., "Linearized Supersonic Unsteady Flow in Cascades," British Aeronautical Research Council, R&M 3811, London, Feb. 1977.

[12]Adamczyk, J. J., and Goldstein, M. E., "Unsteady Flow in a Supersonic Cascade with Subsonic Leading-Edge Locus," *AIAA Journal,* Vol. 16, No. 12, 1978, pp. 1248–1254.

[13]Ni, R. H., "A Rational Analysis of Periodic Flow Perturbation in Supersonic Two-Dimensional Cascade," *Transactions of the American Society of Mechanical Engineers: Journal of Engineering for Power,* Vol. 101, No. 3, 1979, pp. 431–439.

[14]Bendiksen, O. O., and Friedmann, P., "Coupled Bending-Torsion Flutter in Supersonic Cascade," *AIAA Journal,* Vol. 19, No. 6, 1981, pp. 774–781.

[15]Lane, F., "Supersonic Flow Past an Oscillating Cascade with Supersonic Leading-Edge Locus," *Journal of the Aeronautical Sciences,* Vol. 24, No. 1, 1957, pp. 65–66.

[16]Perumal, P. V. K., "Thin Airfoil in Eddy Array and Part-Stalled Oscillating Cascade," Ph.D. Thesis, Stevens Inst. of Technology, Hoboken, NJ, 1976.

[17]Chi, M. R., "Unsteady Aerodynamics in Stalled Cascade and Stall Flutter Prediction," American Society of Mechanical Engineers, ASME Century 2 Aerospace Conference, Paper 80-C2/Aero-1, Aug. 1980.

[18]Goldstein, M. E., Braun, W., and Adamczyk, J. J., "Unsteady Flow in a Supersonic Cascade with Strong In-Passage Shocks," *Journal of Fluid Mechanics,* Vol. 83, Pt. 3, 1977, pp. 569–604.

[19]Namba, M., "Three Dimensional Flows," *AGARD Manual on Aeroelasticity in Axial-Flow Turbomachines, Unsteady Turbomachinery Aerodynamics,* Vol. 1, edited by M. F. Platzer and F. O. Carta, AGARD-AG-298, March 1987, Chapter IV.

[20]Verdon, J. M., "Unsteady Aerodynamics for Turbomachinery Aeroelastic Applications," *Unsteady Transonic Aerodynamics,* edited by D. Nixon, Vol. 120, Progress in Astronautics and Aeronautics, AIAA, Washington, DC, 1989, pp. 287–347.

[21]Verdon, J. M., "Linearized Unsteady Aerodynamics for Turbomachinery Aeroelastic Applications," AIAA/SAE/ASME/ASEE 26th Joint Propulsion Conference, AIAA Paper 90-2355, Orlando, FL, July 16–18, 1990.

[22]Whitehead, D. S., "A Finite Element Solution of Unsteady Two-Dimensional Flow in Cascades," *International Journal for Numerical Methods in Fluids,* Vol. 10, No. 1, 1990, pp. 13–34.

[23]Atassi, H. M., and Akai, T. J., "Aerodynamic and Aeroelastic Characteristics of Oscillating Loaded Cascades at Low Mach Number," *Transactions of the American Society of Mechanical Engineers A: Journal of Engineering for Power,* Vol. 102, No. 2, 1980, pp. 344–356.

[24]Caruthers, J. E., "Aerodynamic Analysis of Cascaded Airfoils in Unsteady Rotational Flow," *Proceedings of the 2nd International Symposium on Aeroelasticity in Turbomachines,* edited by P. Suter, Juris-Verlag, Zurich, Switzerland, 1981, pp. 31–64.

[25]Whitehead, D. S., and Grant, R. J., "Force and Moment Coefficients for High Deflection Cascades," *Proceedings of the 2nd International Symposium on Aeroelasticity in Turbomachines,* edited by P. Suter, Juris-Verlag, Zurich, Switzerland, 1981, pp. 85–127.

[26]Verdon, J. M., and Caspar, J. R., "Development of a Linear Unsteady Aerodynamic Analysis for Finite-Deflection Subsonic Cascades," *AIAA Journal,* Vol. 20, No. 9, 1982, pp. 1259–1267.

[27]Whitehead, D. S., "The Calculation of Steady and Unsteady Transonic Flow in Cascades," Cambridge Univ., Engineering Dept., Rept. CUED/A-Turbo/TR 118, Cambridge, England, UK, 1982.

[28]Verdon, J. M., and Caspar, J. R., "A Linearized Unsteady Aerodynamic Analysis for Transonic Cascades," *Journal of Fluid Mechanics,* Vol. 149, Dec. 1984, pp. 403–429.

[29]Usab, W. J., Jr., and Verdon, J. M., "Advances in the Numerical Analysis of Linearized Unsteady Cascade Flows," *Transactions of the American Society of Mechanical Engineers: Journal of Turbomachinery,* Vol. 113, No. 4, 1991, pp. 633–643.

[30]Hall, K. C., and Verdon, J. M., "Gust Response Analysis for Cascades Operating in Nonuniform Mean Flows," *AIAA Journal,* Vol. 29, No. 9, 1991, pp. 1463–1471.

[31]Caruthers, J. E., and Dalton, W. N., "Unsteady Aerodynamic Response of a Cascade to Nonuniform Inflow," American Society of Mechanical Engineers International Gas Turbine and Aeroengine Congress and Exposition, Paper 91-GT-174, Orlando, FL, June 3–6, 1991.

[32]Hall, K. C., and Crawley, E. F., "Calculation of Unsteady Flows in Turbomachinery Using the Linearized Euler Equations," *AIAA Journal,* Vol. 27, No. 6, 1989, pp. 777–787.

[33]Hall, K. C., and Clark, W. S., "Predictions of Unsteady Aerodynamic Loads in Cascades Using the Linearized Euler Equations on Deforming Grids," AIAA/SAE/ASME/ASEE 27th Joint Propulsion Conference, AIAA Paper 91-3378, Sacramento, CA, June 24-27, 1991.

[34]Joubert, H., "Supersonic Flutter in Axial Flow Compressors," *Proceedings of the Third International Symposium: Unsteady Aerodynamics of Turbomachines and Propellers,* Cambridge Univ. Engineering Dept., Cambridge, England, UK, Sept. 1984, pp. 231–255.

[35]Bölcs, A., Fransson, T. H., and Platzer, M. F., "Numerical Investigation of Unsteady Compressible Flow Through Nozzles and Cascades," *Proceedings of the Fourth International Symposium on Unsteady Aerodynamics and Aeroelasticity of Turbomachines and Propellers,* edited by H. E. Gallus and S. Servaty, Aachen Univ. of Technology, Aachen, Germany, Feb. 1988, pp. 335–355.

[36]Fransson, T. H., and Pandolfi, M., "Numerical Investigation on Unsteady Subsonic Compressible Flows Through an Oscillating Cascade," American Society of Mechanical Engineers 31st International Gas Turbine Conference and Exhibit, Paper 86-GT-304, Dusseldorf, Germany, June 8–12, 1986.

[37]He, L., "An Euler Solution for Unsteady Flows Around Oscillating Blades," *Transactions of the American Society of Mechanical Engineers: Journal of Turbomachinery,* Vol. 112, No. 4, 1990, pp. 714–722.

[38]Huff, D. L., Swafford, T. W., and Reddy, T. S. R., "Euler Flow Predictions for an Oscillating Cascade Using a High Resolution Wave-Split Scheme," American Society of Mechanical Engineers International Gas Turbine and Aeroengine Congress and Exposition, Paper 91-GT-198, Orlando, FL, June 3–6, 1991.

[39]Gerolymos, G. A., Blin, E., and Quiniou, H., "Comparison of Inviscid Computations with Theory and Experiment in Vibrating Transonic Compressor Cascades," American Society of Mechanical Engineers 35th International Gas Turbine and Aeroengine Congress and Exposition, Paper 90-GT-373, Brussels, Belgium, June 11–14, 1990.

[40]Huff, D. L., and Reddy, T. S. R., "Numerical Analysis of Supersonic Flow Through Oscillating Cascade Sections by Using a Deforming Grid," AIAA 25th Joint Propulsion Conference, AIAA Paper 89-2805, Monterey, CA, July 10–12, 1989.

[41]He, L., and Denton, J. D., "Inviscid-Viscous Coupled Solution for Unsteady Flows Through Vibrating Blades, Pt. 1: Description of the Method; Pt. 2: Computational Results," American Society of Mechanical Engineers International Gas Turbine and Aeroengine Congress and Exposition, Papers 91-GT-125 and 91-GT-126, Orlando, FL, June 3–6, 1991.

[42]Siden, L. D. G., Dawes, W. N., and Albraten, P. J., "Numerical Simulation of the Two-Dimensional Viscous Compressible Flow in Blade Cascades Using a Solution Adaptive Unstructured Mesh," *Transactions of the American Society of Mechanical Engineers: Journal of Turbomachinery,* Vol. 112, No. 3, 1990, pp. 311–319.

[43]Siden, L. D. G., "Numerical Simulation of Unsteady Viscous Compressible Flows Applied to Blade Flutter Analysis," American Society of Mechanical Engineers International Gas Turbine and Aeroengine Congress and Exposition, Paper 91-GT-203, Orlando, FL, June 3–6, 1991.

[44]Hodson, H. P., "An Inviscid Blade-to-Blade Prediction of a Wake-Generated Unsteady Flow," American Society of Mechanical Engineers, Paper 84-GT-43, New York, 1984.

[45]Giles, M. B., "Calculation of Unsteady Wake Rotor Interaction," *Journal of Propulsion and Power,* Vol. 4, No. 4, 1988, pp. 356–362.

[46]Koya, M., and Kotake, S., "Numerical Analysis of Fully Three-Dimensional Periodic Flows Through a Turbine Stage," *Transactions of the American Society of Mechanical Engineers: Journal of Engineering for Gas Turbines and Power,* Vol. 107, No. 1, 1985, pp. 945–952.

[47]Fourmaux, A., "Unsteady Flow Calculation in Cascades," American Society of Mechanical Engineers International Gas Turbine Conference and Exhibit, Paper 86-GT-178, Dusseldorf, Germany, June 8–12, 1986.

[48]Lewis, J. P., Delaney, R. A., and Hall, E. J., "Numerical Prediction of Turbine Vane-Blade Interaction," AIAA 23rd Joint Propulsion Conference, AIAA Paper 87-2149, San Diego, CA, June 29–July 2, 1987.

[49]Giles, M. B., "Stator/Rotor Interaction in a Transonic Turbine," *Journal of Propulsion and Power,* Vol. 6, No. 5, 1990, pp. 621–627.

[50]Rai, M. M., "Navier-Stokes Simulations of Rotor-Stator Interaction Using Patched and Overlaid Grids," *Journal of Propulsion and Power,* Vol. 3, No. 5, 1987, pp. 387–396.

[51]Rai, M. M., "Three-Dimensional Navier-Stokes Simulations of Turbine Rotor-Stator Interaction; Pt. 1—Methology, Pt. 2—Results," *Journal of Propulsion and Power,* Vol. 5, No. 3, 1989, pp. 305–319.

[52]Giles, M. B., and Haimes, R., "Validation of a Numerical Method for Unsteady Flow Calculations," American Society of Mechanical Engineers International Gas Turbine and Aeroengine Congress and Exposition, Paper 91-GT-271, Orlando, FL, June 3–6, 1991.

[53]Rai, M. M., and Dring, R. P., "Navier-Stokes Analyses of the Redistribution of Inlet Temperature Distortions in a Turbine," *Journal of Propulsion and Power,* Vol. 6, No. 3, 1990, pp. 276–282.

[54]Krouthen, B., and Giles, M., "Numerical Investigation of Hot Streaks in Turbines," *Journal of Propulsion and Power,* Vol. 6, No. 6, 1990, pp. 769–776.

[55]Dorney, D. J., Davis, R. L., Edwards, D. E., and Madavan, N. K., "Unsteady Analysis of Hot Streak Migration in a Turbine Stage," AIAA 26th Joint Propulsion Conference, AIAA Paper 90-2354, Orlando, FL, July 16–18, 1990.

[56]Aris, A., *Vectors, Tensors and the Basic Equations of Fluid Mechanics,* Prentice-Hall, Englewood Cliffs, NJ, 1962.

[57]Melnik, R. E., "Turbulent Interactions on Airfoils at Transonic Speeds—Recent Developments," *AGARD Symposium on Computation of Viscous-Inviscid Flows,* AGARD-CP-291, Paper 10, 1980.

[58]Lock, R. C., and Firmin, M. C. P., "Survey of Techniques for Estimating Viscous Effects in External Aerodynamics," *Proceedings of the IMA Conference on Numerical Methods in Aeronautical Fluid Dynamics,* edited by P. L. Roe, Academic Press, New York, 1982, pp. 337–430.

[59]Cebeci, T., and Smith, A. M. O., *Analysis of Turbulent Boundary Layers,* Academic Press, New York, 1974, pp. 211–239.

[60]Baldwin, B. S., and Lomax, H., "Thin-Layer Approximation and Algebraic Model for Separated Turbulent Flow," AIAA 16th Aerospace Sciences Meeting, AIAA Paper 78-257, Huntsville, AL, Jan. 16–18, 1978.

[61]Giles, M. B., "Nonreflecting Boundary Conditions for Euler Equation Calculations," *AIAA Journal,* Vol. 28, No. 12, 1990, pp. 2050–2058.

[62]Erdos, J. I., Alzner, E., and McNally, W., "Numerical Solution of Periodic Transonic Flow Through a Fan Stage," *AIAA Journal,* Vol. 15, No. 11, 1977, pp. 1559–1568.

[63]Verdon, J. M., "The Unsteady Flow in the Far Field of an Isolated Blade Row," *Journal of Fluids and Structures,* Vol. 3, No. 2, 1989, pp. 123–149.

[64]Kovasznay, L. S. G., "Turbulence in Supersonic Flow," *Journal of the Aeronautical Sciences,* Vol. 20, No. 10, 1953, pp. 657–674.

[65]Goldstein, M. E., "Unsteady Vortical and Entropic Distortions of Potential Flows Round Arbitrary Obstacles," *Journal of Fluid Mechanics,* Vol. 89, Pt. 3, 1978, pp. 433–468.

[66]Caspar, J. R., "Unconditionally Stable Calculation of Transonic Potential Flow Through Cascades Using an Adaptive Mesh for Shock Capture," *Transactions of the American Society of Mechanical Engineers: Journal of Engineering for Power,* Vol. 105, No. 3, 1983, pp. 504–513.

[67]Whitehead, D. S., and Newton, S. G., "A Finite Element Method for the Solution of Two-Dimensional Transonic Flows in Cascades," *International Journal for Numerical Methods in Fluids,* Vol. 5, No. 2, 1985, pp. 115–132.

[68]Goldstein, M. E., "Turbulence Generated by the Interaction of Entropy Fluctuations with Non-Uniform Mean Flows," *Journal of Fluid Mechanics,* Vol. 93, Pt. 2, 1979, pp. 209–224.

[69]Atassi, H. M., and Grzedzinski, J., "Unsteady Disturbances of Streaming Motions Around Bodies," *Journal of Fluid Mechanics,* Vol. 209, Dec. 1989, pp. 385–403.

[70]Verdon, J. M., "The Unsteady Aerodynamic Response to Arbitrary Modes of Blade Motion," *Journal of Fluids and Structures,* Vol. 3, No. 3, 1989, pp. 255–274.

[71]Williams, M. H., "Linearization of Unsteady Transonic Flows Containing Shocks," *AIAA Journal,* Vol. 17, No. 4, 1979, pp. 394–397.

[72]Ehlers F. E., and Weatherill, W. H., "A Harmonic Analysis Method for Unsteady Transonic Flow and Its Application to the Flutter of Airfoils," NASA CR 3537, May 1982.

[73]Smith, T. E., "Aerodynamic Stability of a High-Energy Turbine Blade," AIAA/SAE/ASME/ASEE 26th Joint Propulsion Conference, AIAA Paper 90-2351, Orlando, FL, July 16–18, 1990.

[74]Smith, T. E., and Kadambi, J. R., "The Effect of Steady Aerodynamic Loading on the Flutter Stability of Turbomachinery Blading," American Society of Mechanical Engineers International Gas Turbine and Aeroengine Congress and Exposition, Paper 91-GT-130, Orlando, FL, June 3–6, 1991.

[75]Suddhoo, A., and Stow, P., "Simulation of Inviscid Blade-Row Interaction Using a Linearized Potential Code," AIAA/SAE/ASME/ASEE 26th Joint Propulsion Conference, AIAA Paper 90-1916, Orlando, FL, July 16–18, 1990.

[76]Jang, H. M., Platzer, M. F., Ekaterinaris, J. A., and Cebeci, T., "Essential Ingredients for the Computation of Steady and Unsteady Blade Boundary Layers," American Society of Mechanical Engineers 35th International Gas Turbine and Aeroengine Congress and Exposition, Paper 90-GT-160, Brussels, Belgium, June 11–14, 1990.

[77]Verdon, J. M., Barnett, M., Hall, K. C., and Ayer, T. C., "Development of Unsteady Aerodynamic Analyses for Turbomachinery Aeroelastic and Aeroacoustic Applications," NASA Lewis Research Center, CR 4405, Cleveland, OH, Oct. 1991.

[78]Caspar, J. R., and Verdon, J. M., "Numerical Treatment of Unsteady Subsonic Flow Past an Oscillating Cascade," *AIAA Journal,* Vol. 19, No. 12, 1981, pp. 1531–1539.

[79]Ni, R. H., and Sisto, F., "Numerical Computation of Nonstationary Aerodynamics of Flat Plate Cascades in Compressible Flow," *Transactions of the American Society of Mechanical Engineers: Journal of Engineering for Power,* Vol. 98, No. 2, 1976, pp. 165–170.

[80]Ni, R. H., "A Multiple Grid Scheme for Solving the Euler Equations," *AIAA Journal,* Vol. 20, No. 11, 1981, pp. 1565–1571.

[81]Fransson, T. H., and Suter, P., "Two-Dimensional and Quasi Three-Dimensional Experimental Standard Configurations for Aeroelastic Investigations in Turbomachine-Cascades," Ecole Polytechnique Federale de Lausanne, Rept. LTA-TM-83-2, Lausanne, Switzerland, Sept. 1983.

[82]Huff, D. L., private communication, Sept. 1991.

[83]Bölcs, A., and Fransson, T. H., "Aeroelasticity in Turbomachines Comparison of Theoretical and Experimental Cascade Results," Communication du Laboratoire de Thermique Applique et de Turbomachines, Nr. 13, Ecole Polytechnique Federale de Lausanne, Lausanne, Switzerland, 1986.

[84]Fransson, T. H., and Verdon, J. M., "Updated Report on 'Standard Configurations' for the Determination of Unsteady Flow Through Vibrating Axial-Flow Turbomachine Cascades," Sixth International Symposium on Unsteady Aerodynamics, Aeroacoustics, and Aeroelasticity of Turbomachines and Propellers, Univ. of Notre Dame, Notre Dame, IN, Sept. 15–19, 1991 (proceedings to be published by Springer-Verlag, New York).

[85]Carta, F. O., "Unsteady Aerodynamics and Gapwise Periodicity of Oscillating Cascaded Airfoils," *Transactions of the American Society of Mechanical Engineers: Journal of Engineering for Power,* Vol. 105, No. 3, 1983, pp. 565–574.